



FACULTY OF INFORMATION TECHNOLOGY AND ELECTRICAL ENGINEERING
DEGREE PROGRAMME IN ELECTRONICS AND COMMUNICATIONS ENGINEERING

MASTER'S THESIS

The improvement of 5G massive MIMO antenna array port-to-port isolation

Author	Harri Joonas
Supervisor	Ping Jack Soh
Second Examiner	Risto Vuhtoniemi
Technical Advisor	Tomi Haapala

April 2023

Joona H. (2023) The improvement of 5G massive MIMO antenna array port-to-port isolation. University of Oulu, Faculty of Information Technology and Electrical Engineering, Degree Programme in Electronics and Communications Engineering. Master's Thesis, 57 p.

ABSTRACT

In this thesis, the phenomenon of mutual coupling in 5G mMIMO base station antenna array is studied and a solution to improve port-to-port isolation is proposed. Mutual coupling occurs when antennas are placed close to each other in modern base station antenna arrays. Basically, it causes other antennas to absorb part of the antenna's radiated energy or rescatter a portion of the incident energy in various directions, allowing them to act as secondary transmitters. The absorbed energy by other antenna changes an array radiation pattern, array manifold and radiators input impedance changed. This is not a desirable phenomenon because the other antennas' absorbed energy is not radiated as designed and change in input impedance causes mismatches. So, mutual coupling lowers antenna array efficiency and performance in transmitter and receiver.

The initial antenna array design in this work is Nokia's own model, operating in the frequency band of 3.3–3.8 GHz. It is already in the production and deployment phase to the field for customers. The aim of the work was to improve port-to-port isolation from -18.74 dB to -30 dB while maintaining all other design parameters for matching and radiation properties. To do this, antenna mutual coupling is studied and simulated in the original design with the electromagnetic simulation tool Ansys HFSS. The simulation cases are divided into smaller models, based on how coupling occurs in the design. Root causes for restricting the isolation performance are observed and a proposed method for improved port-to-port isolation is illustrated. To verify the correct radiation performance for the proposed method, radiation results are post-processed with MATLAB. Finally, the results are analysed based on the base station antenna standards and compared to the initial design. This thesis provided a 2.84 dB for port-to-port isolation improvement while meeting all other design specifications.

Key words: phased antenna array, dual polarized antenna, mutual coupling, electromagnetic simulation software.

Joona H. (2023) Portista porttiin välisen isolaation parantaminen 5G mMIMO antenniryhmässä. Oulun yliopisto, tieto- ja sähkötekniikan tiedekunta, elektronikan ja tietoliikennetekniikan tutkinto-ohjelma. Diplomityö, 57 p.

TIIVISTELMÄ

Tässä diplomityössä tutkitaan antennien välistä keskinäistä kytkeytymistä 5G mMIMO-tukiasema-antenniryhmässä ja esitellään ratkaisu portista porttiin välisen isolaation parantamiseksi. Antennien välinen keskinäinen kytkeytyminen tapahtuu, kun ne ovat lähellä toisiaan moderneissa tukiasema-antenniryhmissä. Sen takia toiset antennit absorboivat osan yhden antennin lähettämästä energiasta tai uudelleen sirottavat sen useisiin suuntiin aiheuttaen niiden toimimisen sekundäärisinä lähettiminä. Toisten antennien absorboima energia muuttaa niiden säteilykuvioita, jännitteitä ja tuloimpedanssia. Tämä ei ole toivottu ilmiö, koska toisten antennien absorboima energia ei ole lähetetty alkuperäisestä säteilijästä kuten on suunniteltu, ja tuloimpedanssin muutos aiheuttaa antenneihin epäsovutusta. Antennien välinen kytkeytyminen siis huonontaa antenniryhmän tehokkuutta ja suorituskykyä sekä lähettimessä että vastaanottimessa.

Työn alkuperäinen antenniryhmämalli on Nokian kehittämä ja toimii 3.3–3.8 GHz taajuuskaistalla. Se on jo tuotanto- ja käyttöönottovaiheessa kentällä asiakkaille. Tämän työn tavoite on parantaa portista porttiin välistä isolaatiota -18.74 dB:stä -30 dB:iin säilyttäen samalla kaikki muut suunnitteluparametrit sovitukselle ja säteilyominaisuuksille. Tämän saavuttamiseksi antennien keskinäistä kytkentää tutkitaan ja simuloidaan alkuperäisessä mallissa sähkömagneettisella simulointityökalulla, Ansys HFSS:llä. Simulaatiotapaukset on jaettu pienempiin osiin sen mukaan, miten antennien välinen keskinäiskytkentä tapahtuu alkuperäisessä mallissa. Isolaation suorituskyvyn rajoittamisen juurisyyt esitellään ja ehdotettu menetelmä porttien välisen eristyksen parantamiseksi mallinnetaan ja simuloidaan. Ehdotetun menetelmän säteilyominaisuuksien tarkistamiseksi tulokset jälkikäsitellään MATLAB-ohjelmistolla. Lopuksi säteilytuloksia analysoidaan tukiaseman antennistandardien perusteella ja verrataan alkuperäiseen malliin. Tässä työssä saavutetaan 2.84 dB:n parannus portista porttiin isolaatioon samalla saavuttaen kaikki muut suunnitteluspesifikaatiot.

Avainsanat: vaiheistetut antenniryhmät, kaksoispolarisoitu antenni, keskinäiskytkentä, sähkömagneettinen simulointiohjelmisto.

TABLE OF CONTENTS

ABSTRACT	2
TIIVISTELMÄ.....	3
TABLE OF CONTENTS	4
FOREWORD	6
LIST OF ABBREVIATIONS AND SYMBOLS	7
1 INTRODUCTION	9
2 RF SYSTEM.....	11
2.1 RF system.....	11
2.2 Frequency spectrum	11
2.3 Wireless concept of base stations	12
3 5G TDD BASE STATION	13
3.1 5G frequency spectrum	13
3.2 Duplexing	13
3.3 5G TDD architecture	14
3.4 Microstrip antenna.....	15
3.5 Antenna array	16
3.6 Massive MIMO	17
3.7 Beamforming.....	18
4 ANTENNA THEORY	19
4.1 Electromagnetic radiation	19
4.2 Antenna definition.....	20
4.3 Radiation mechanism	21
4.4 Aspects of propagation.....	21
4.4.1 Free-space propagation.....	21
4.4.2 Reflection, diffraction and scattering	22
4.5 Input impedance	22
4.6 Radiation pattern	23
4.7 Scattering parameters	23
4.8 Mutual coupling	24
4.8.1 Transmission mode.....	24
4.8.2 Reception mode	25
4.9 Driving impedance	26
4.10 Mutual coupling in the array microstrip antennas.....	27
4.11 Cross polar discrimination	27
4.12 Decoupling techniques in antenna arrays	28
5 OBSERVATION OF ANTENNA MUTUAL COUPLING	29
5.1 Initial antenna array design	29
5.1.1 Air insulated dual polarized balanced probe feed microstrip antenna	30
5.1.2 Antenna array design	31
5.1.3 Initial results for antenna matching and port-to-port isolation.....	32
5.2 Root causes of implementation for antenna coupling	35

5.2.1	Antenna mutual coupling in small array	36
5.2.2	Behaviour of electromagnetic fields in small array.....	38
5.2.3	Impact of phased feed network.....	39
5.2.4	Antenna feedline location and orientation.....	43
6	PROPOSED METHOD TO IMPROVE PORT-TO-PORT ISOLATION.....	46
6.1	Implementation of proposed method to improve isolation	46
6.2	S-parameter results	47
6.3	Radiation results	50
7	DISCUSSION.....	54
8	SUMMARY.....	56
9	REFERENCES	57

FOREWORD

This Master's thesis was done at Nokia Solutions and Networks in the Oulu Antenna & Filter team in the product development organization. First of all, I want to thank my line manager, M.Sc. (MBA) Jari Lapinlampi, for the opportunity to do this thesis, which provided me with a huge learning opportunity of modern 5G base station mMIMO phased antenna array design. Then, I want to show my gratitude for my technical advisor, M.Sc. (Tech) Tomi Haapala, for his expert guidance during the work. Additionally, I want to thank M.Sc. (Tech) Heikki Korva for comments and advices and the whole Nokia's Antenna team for their support during the work. Also, I want to thank my supervisor D.Sc. (Tech) Ping Jack Soh and second examiner Lic.Sc. (Tech) Risto Vuhtoniemi for reading and reviewing this thesis. Finally, I want to thank my fellow students, family and girlfriend Alisa for huge support during my studies at University.

Oulu, April 5, 2023

Harri Joona

LIST OF ABBREVIATIONS AND SYMBOLS

1G	First generation
2G	Second generation
3D	Three-dimensional
3G	Third generation
3GPP	3rd Generation Partnership Project
4G	Fourth generation
5G	Fifth generation
AF	Array factor
BS	Base station
CPD	Cross polar discrimination
DL	Downlink
EM	Electromagnetic
eMBB	enhanced mobile broadband
FDD	Frequency division duplex
GPS	Global Positioning System
HD	High Definition
HFSS	High Frequency Simulation Software
IoT	Internet of Things
IP	Internet Protocol
LNA	Low noise amplifier
LTE	Long Term Evolution
MIMO	Multiple-Input and Multiple-Output
mMIMO	massive Multiple-Input and Multiple-Output
mmWave	millimetre wave
PA	Power amplifier
PCB	Printed circuit board
RF	Radio frequency
RX	Receive
S-parameter	Scattering parameter
TDD	Time division duplex
TRX	Transceiver
TX	Transmit
UHD	Ultra-High Definition
UL	Uplink
A_{eff}	effective aperture area
B	bandwidth
\mathbf{B}	magnetic flux density
C	capacity
C_{ij}	mutual coupling between the i th and j th antennas
\mathbf{D}	electric flux density
\mathbf{E}	electric field vector
dB	decibel
dBi	the gain of an antenna compared to the gain of an isotropic antenna
d_{ij}	distance between the i th and j th antennas
d_x	antenna spacing in column

d_y	antenna spacing in row
f	frequency
G	antenna gain
G_a	antenna array gain
G_r	antenna gain at receiver
G_t	antenna gain at transmitter
Gbps	giga bit per second
GHz	giga hertz
H	magnetic field vector
I_0	excitation coefficient of an array
J	current density
k	angular wavenumber of an array
kbit/s	kilobits per second
M	number of rows in an array
Mbit/s	megabits per second
MHz	mega hertz
N	number of columns in an array
N_e	number of antennas in the array
P_r	receive power
P_t	transmit power
r	radial distance
R_L	loss resistance
R_r	antenna radiation resistance
S	power density
S_{ij}	scattering parameter of port i to port j
S/N	signal-to-noise-ratio
t	time
V_j^+	voltage fed to port j
V_i^-	reflected wave coming from port i
V_g	voltage generator voltage
X_A	antenna radiation reactance
Z_A	antenna impedance
Z_g	voltage generator impedance
Z_T	transmission line impedance
α	parameter for coupling level
β_x	progressive phase shift between antenna along the x-axis
β_y	progressive phase shift between antenna along the y-axis
ϵ_r	relative permittivity
Θ	elevation angle
λ	wavelength
ρ	charge density
φ	azimuth angle

1 INTRODUCTION

Telecommunication for commercial applications was started when the advanced mobile telephony system was launched into operation in the USA in 1983. At first, only voice data was delivered from user to another, which limited the needed amount of data delivery to 2.4 kbit/s. A great deal of improvement has been made after that and developments have been growing explosively. On average, every 10 years a new telecommunication standard has been launched, which has revolutionized the world and connected people with new ways regardless of time or place. While 1G leaned on a fully analog communication technology, for 2G digital communication technology was utilized. This enabled people to communicate using text messages and regular voice calls with a better quality and security level with 384 kbit/s data rate. In turn, 3G brought web browsing, voice over IP and video streaming to mobile terminals, which all were remarkable milestones for the telecommunication industry. Those features were enabled by utilizing a data packet-based communication technology, which was a big innovation in 3G. The next step was to improve it so much that the data rate could be increased to hundreds of megabits per second with wide bandwidth. This enabled mobile gaming and HD streaming via a wireless connection for 4G. It was developed even further and is known as Long Term Evolution (LTE). It enabled data rates up to 1000 Mbit/s for downlink and 500 Mbit/s for uplink in an optimal situation. [1]

After LTE reached the point that only a few improvements in data rates and small amounts of new spectrum could be expected, the telecommunication industry was heading to develop 5G next. It is planned to enable brand new services, ecosystems, revenues and better end-user experiences than 4G. For the general mobile handset user, it will be enabling such features like ultra-high definition (UHD) streaming and the usage of virtual reality and high-definition three-dimensional (3D) videos, which will be the evolution of enhanced mobile broadband (eMBB) data services. However, the key feature of 5G for the industry is to enable communication of things. At best, 5G could be the fourth industrial revolution for the industry that enables the internet of things (IoT) to factories, hospitals, cities and homes. Communication between a massive number of things would be done with high reliability, low latency, low cost and high data rate. [1]

The number of subscriptions on telecommunication services has passed the population of the world several years ago already. [2] So, it is safe to say that almost everyone is using telecommunication systems in these days. The new ways to use telecommunication systems that have been found during past decades have set higher and higher requirements for the communication link providers ergo base station (BS). From 1G to 5G, the number of used antennas in base station have grown greatly. This has been a natural development, since the function of antenna diversity was found already in 1931 by RCA engineers Harold H. Beverage and Harold O. Peterson. They found that combining signals from two different receivers can improve the audio quality in radio broadcasts. [3] In the first cellular generations, this was utilized in the receiver (RX) of base stations to reduce effect of multipath fading. When the attempts were made to increase data rates for LTE, the use of antenna array became common in the industry and multiple antennas were used for the first time in base stations both in transmission and reception. [4]

LTE enabled high data rates for wireless communication already and the base station was designed so that one cell had one wide radiation beam per cell. One of the advantages for 5G base station compared to LTE is that the antenna radiation pattern is narrower and a higher antenna gain is achieved directly to user. In 5G, the base station is directly radiating and closely based array of

antennas are used to create narrow radiation pattern. Radiation can be formed to the desired direction using phased antenna feeding, which is called beamforming. It improves channel capacity greatly since resources of each cell can be reused to many users with mMIMO beamforming. [4] The usage of massive MIMO has been a key development for 5G although the increased operation frequencies increase path loss, but with mMIMO and beamforming the 5G cell size in 3.5 GHz frequency band should be able to match the 4G system cell size. [5]

5G standardization has been in development since 2016 by 3GPP, and the first commercial 5G network has been deployed for sub-6 GHz in 2019. [6] This sub-6 GHz spectrum, where low 5G bands are allocated, is planned to serve wide area coverage needs with potentially a few Gbps data rates. The 5G base station mMIMO antenna array in sub-6 GHz has nearly a hundred antennas placed close to each other. While the antennas are placed close to each other to create a narrow beam and beamforming, a phenomenon called antenna mutual coupling occurs. This mutual coupling restricts antenna performance, and the solutions for improving isolation between antenna ports are researched in this thesis work.

The antenna array design of this thesis is the model of Nokia, and it is in the initial state of the design. It is already in the production and deployment phase. The design covers the 3.3–3.8 GHz band, but is simplified to be speed up simulation analysis. The antenna array model contains 96 antennas distributed into 8 columns and 12 rows, with 32 subarrays, which each has 3 antennas and is fed through individual transceiver (TRX) ports. A single antenna in the antenna array design is an dual-polarized microstrip antenna, which means that every antenna is fed in two different ports to create $\pm 45^\circ$ dual polarizations. Two radiating elements are combined into one antenna to provide polarization diversity. The usage of dual polarized antenna produces internal coupling in the antenna, and it affects the full array port-to-port isolation and also needs to be analysed.

The aim of this thesis is to illustrate the occurrence of mutual coupling in the antenna array, examine the root causes of implementation restricting isolation performance and, finally, to propose method to isolate it. The main goal for port-to-port isolation is to improve it from -18.74 dB to -30 dB while maintaining all the radiation properties for antenna array. This could become beneficial for the entire antenna array's overall performance and it might make it possible to decrease antenna array within the azimuth direction beneath 0.5λ , which would benefit the beam steering capability. Furthermore, it could make it possible to remove the circulator from the architecture. Eliminating the circulator would arrange requirements also to other transceiver blocks such as the power amplifier (PA) in transmitter (TX) chain and the low noise amplifier (LNA) in RX chain, but this thesis will be concentrating on enhancing only the overall performance of antenna array. To examine the functionality of the antenna array and mutual coupling, it is modelled and simulated using the electromagnetic (EM) simulator Ansys HFSS. Because the phenomenon of mutual coupling needs to be understood completely to fulfil the goals of this thesis, the simulations are divided based on how coupling is occurring in the design to observe the root causes for antenna array mutual coupling. Based on the restricting parameters for mutual coupling, the method to improve the port-to-port is simulated experimentally. Finally, the method to improve port-to-port is proposed. The radiation properties of the initial and proposed methods are compared based on the base station antenna standards to verify the radiation performance of the proposed method and to analyse how radiation properties are changed while array port-to-port isolation is improved.

2 RF SYSTEM

The number of different kinds of radio frequency (RF) systems used in wireless communication has grown greatly. Almost every device nowadays has an RF unit in it. The toys of children to more complex electronics, such as mobile phones, wireless earphones, door openers, remote-piloted vehicle controls, cars and GPS systems, have RF parts to provide wireless connectivity. Different devices have various requirements for transceivers, although the nature of the usage for the system determines them. Some systems might just need to send an RF signal for a few meters away and other systems do it all the way from Earth to space. For people communicating with each other with cellular devices, base stations are providing a path for data traffic. This chapter examines the basic principles regarding the base station as an RF system and its functionality. [7]

2.1 RF system

In the RF system, the information signal is sent from the transmitter to the receiver regardless of the place or the time of the devices. The simple concept of the one-way RF system is illustrated in Figure 1. The function of the transmitter is to handle the information signal such a way that it is at a suitable power level to be sent from the transmit antenna through the transmitting medium to the receive antenna. In an ideal world, the signal would be at the same power level in the receive antenna as it was sent from the transmit antenna, but it is losing more and more strength while it travels through a medium. The medium is usually air, but it can be also liquid or solid material. The receive antenna captures the RF signal sent from the transmitter. The receiver amplifies this signal and extracts information from it. In the base station, this function is utilized in two ways, so it is acting as transceiver. [7]

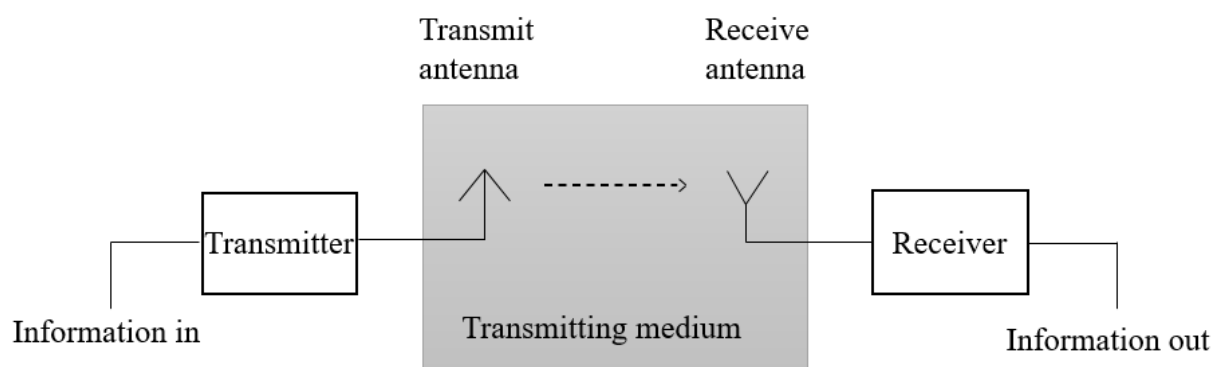


Figure 1. The simple concept of the RF system. [7]

2.2 Frequency spectrum

The RF system always requires antenna in the transmitter and receiver as illustrated in Figure 1. In the antenna design, the size of the antenna depends on its operating frequency. Designing antennas for very low frequencies would require antennas to be too large to be practical in user devices and, therefore, the use of low frequencies is impractical. However, while designing the RF system for higher frequencies, antennas are made smaller, but power losses and the Doppler fading increases so the operating range of the system will be much smaller. With these

constraints, the useful RF frequency spectrum is restricted and the planning of the operating frequency for different products becomes important. [7]

2.3 Wireless concept of base stations

The idea of cellular connectivity is to provide a wireless connection from one user to another regardless of their space or time. Wireless networks are built in such a way that all populated areas are covered. Each base station covers one restricted area called cell. If the user moves away from one coverage area of one base station, the user enters another cell, which is covered with another base station. The cells are designed such a way that they do not interfere with each other and are same size cubes. A group of cells form one cluster, where base stations are connected to each other and to central computer with wire, is illustrated in Figure 2. This enables preventing the loss of communication while the user is moving from one cell to another while the central computer uses information of the user's location to decide which base station the user should connect to in order to remain within the wireless connection. In such a cluster of base stations, system capacity is increased compared to a solution where one base station is covering a cluster with the same size, since cells can belong to different clusters and all frequencies can be used in each cluster. [7]

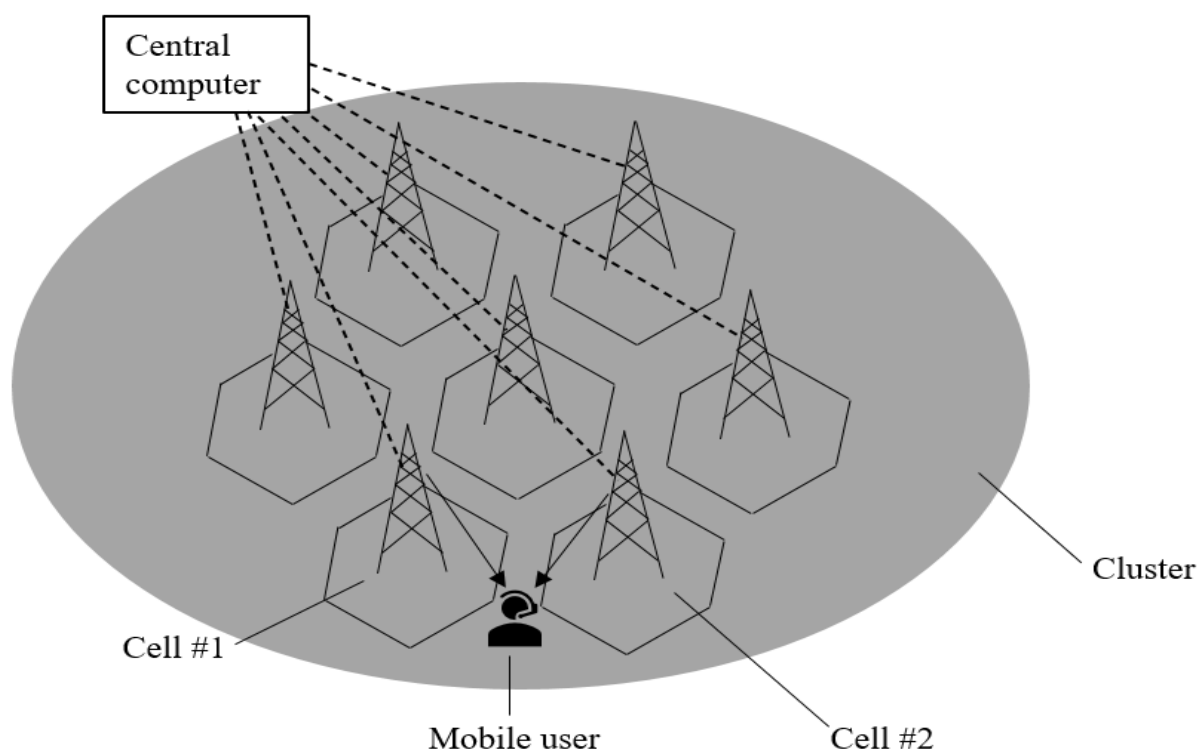


Figure 2. A cluster of base station cells. [7]

3 5G TDD BASE STATION

This thesis concentrates on the research on the mMIMO antenna array port-to-port isolation improvement of the 5G TDD base station, operating in the 3.5 GHz frequency band. This frequency spectrum is planned to operate in the same cell size as LTE, but with improved capacity, data rates, spectral efficiency with power of mMIMO beamforming. In this chapter, the 5G frequency spectrum, 5G TDD architecture, mMIMO antenna array and used antenna type are covered.

3.1 5G frequency spectrum

The deployment of 5G to sub-6 GHz has already started four years ago. These low frequencies are where a wide coverage area can be reached. Frequencies below 2 GHz are mainly already used by other systems, but there have been plans to reallocate some frequencies below 1 GHz for the use of 5G to achieve high coverage areas, which have been reached with 2G and 3G systems. However, the main frequency spectrum below 6 GHz for 5G is going to be 3.5 GHz. This frequency area is useful since it is available internationally and provides a high amount of frequency range. It can be seen from Figure 3. As frequencies get higher, coverage gets lower and lower because the path loss increases. Frequencies from 24 GHz and above are allocated to mmWave. Those are planned to cover small, but high-capacity areas like airports, event stadiums and city centres. In mmWave, very high data rates and capacity are reached. However, in this thesis we will concentrate on the 3.5 GHz band. [5]

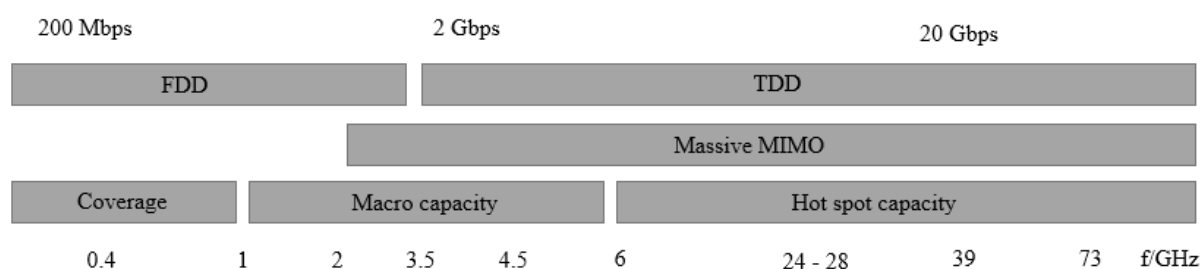


Figure 3. Possible allocation for 5G frequency spectrum. [5]

3.2 Duplexing

A modern base station is designed so that it is using the same antenna array for transmission and reception. This can be achieved with duplexing. The options for duplexing are frequency division duplexing (FDD) and time division duplexing (TDD) as illustrated in Figure 4. FDD is used mainly in sub-3.5 GHz systems separating the uplink (UL) and the downlink (DL) of the base station in its own frequency bands so that both channels have equal bandwidth. The UL and DL bands need to be separated with a guard band of more than the coherence bandwidth to disable the interference between the transmitter and the receiver. This concept provides full data capacity to both the UL and DL at any time, but can lead to unused frequency band if communication traffic is not symmetric. The operation of the TDD architecture is based on a time division duplex, which uses a single carrier frequency for uplink and downlink while

dividing those in time. This provides the same bandwidth usage for transmission and reception. [7]

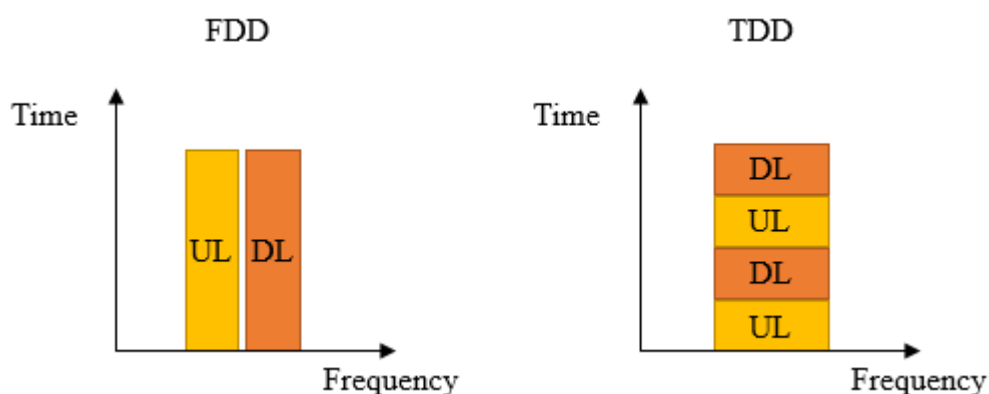


Figure 4. A comparison of FDD and TDD.

3.3 5G TDD architecture

The RF front-end of the 5G TDD base station transceiver is illustrated in Figure 5. This architecture uses the same antennas for transmission and reception, and the operations are separated in time. Every antenna port is connected to its own TRX chain. In the block diagram of Figure 5, the functionality of the circulator is to ensure the isolation of the transmitter and the receiver. The circulator is useful for this since its function is to lead the input only to the first output, but not to the second output. When the base station is in transmitting mode, the power amplifier (PA) amplifies the low-level RF signal to a high power level. The function of the coupler is to provide the output of the PA to feedback and transmission. The feedback is used for the predistortion of the PA to provide a linear output signal for the PA. Circulator leads a high power RF signal from the coupler to the filter. The filter is band pass filter, which passes the signal in the wanted frequency band and rejects out of a band signal, possibly produced by the PA. Circulator leads possible reflections due to mismatches and antenna mutual coupling in the antenna port to RX chain, where the switch is turned to termination. In the reception mode of the base station, the circulator conducts received a weak RF signal from the antenna port to the low noise amplifier (LNA) of the RX chain and the LNA amplifies it for the RX output. During reception, the circulator isolates the TX chain from the received RF signal. Each antenna port has its own TRX chain.

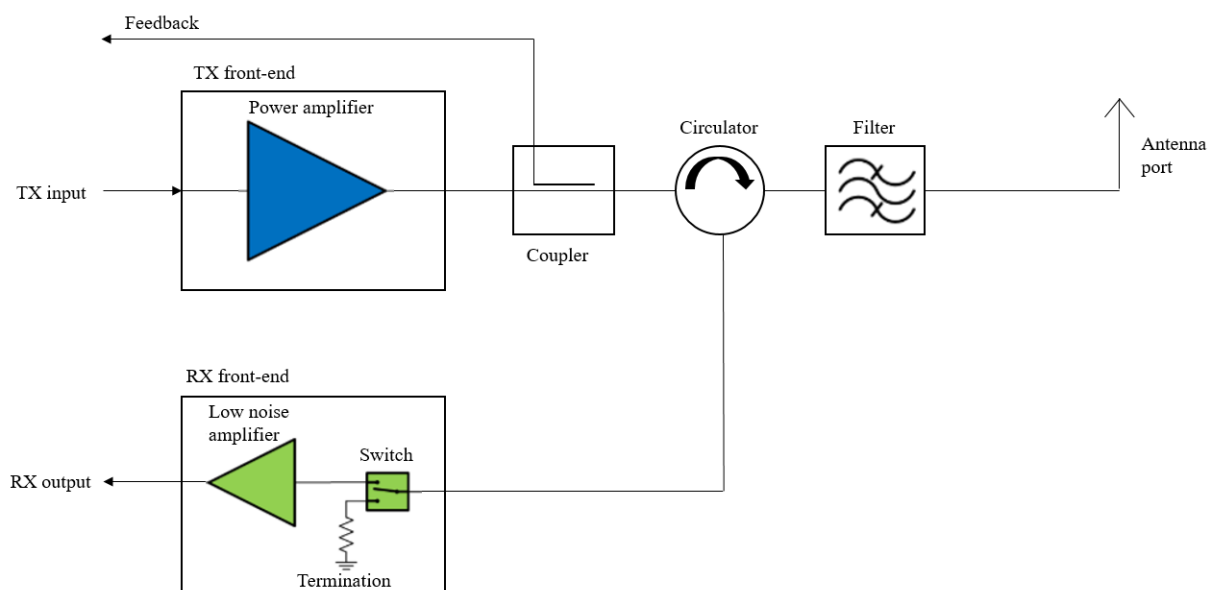


Figure 5. A high-level block diagram of TRX front-end architecture.

3.4 Microstrip antenna

Base stations should be as light and inexpensive as possible, and the load of the wind for the base station also needs to be considered while designing antennas for it. The ease of fabrication, high performance and low-profile structure are figures of merits for the microstrip antenna, so is it widely used in the wireless industry. Microstrip antennas are usually called patch antennas. The name refers to the radiating structure, which are placed a small distance above the ground plane as can be seen from Figure 6. Even though the patch can be rectangular, circular, triangular or anything between, a rectangular patch is most common nowadays in the base station antenna design. The substrate is placed between the patch and the ground plane, and it handles the grounding of the radiating patch antenna. Choosing the suitable substrate material for the microstrip is important since the dielectric constant ϵ_r affects the antenna performance. The patch antenna is designed for certain operation frequency and radiation characteristics. This is done by choosing the suitable length, width and thickness of the patch, and the dimensions and material of the substrate also need to be taken into consideration while designing antenna. Finally, the matching of the feedline for the suitable impedance needs to be done for efficient radiation performance. [8]

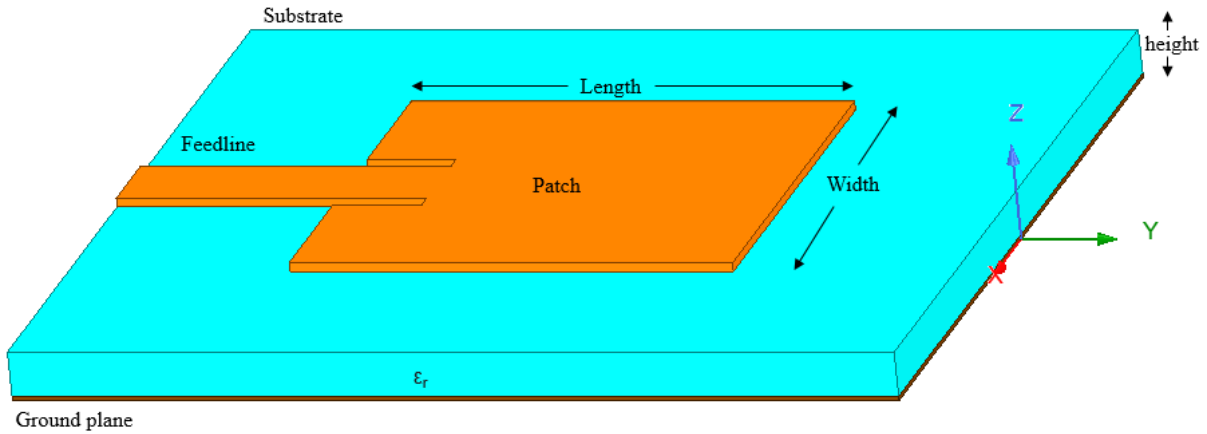


Figure 6. Microstrip patch antenna. [8]

3.5 Antenna array

The analysis of a single antenna commonly produces a wide radiation pattern with low gain. A modern 5G base station is designed to have a narrow radiation pattern with high gain. This is accomplished with planar antenna array as illustrated in Figure 7. Antennas placed close to each other already modify the radiation pattern of the whole array by interfering with each other. The radiation to the desired direction is intensified and the radiation to other directions gets cancelled. For designing an antenna array, this would ideally be enough, but in reality, antennas have to be fed with a suitable phase difference to produce a narrow radiation pattern for the whole antenna array. With this technique, the radiation beam can be formed to any point in space within the limits of a single antenna radiation pattern, which enables beam steering directly to the user connecting to the base station.

In Figure 7, there are antennas placed in the planar array along a rectangular grid in the spherical coordinate system with N columns and M rows. Antenna spacing in the column is represented using d_x and d_y for rows. The direction of the radiation beam is defined with the elevation angle θ and azimuth angle ϕ to radial distance r .

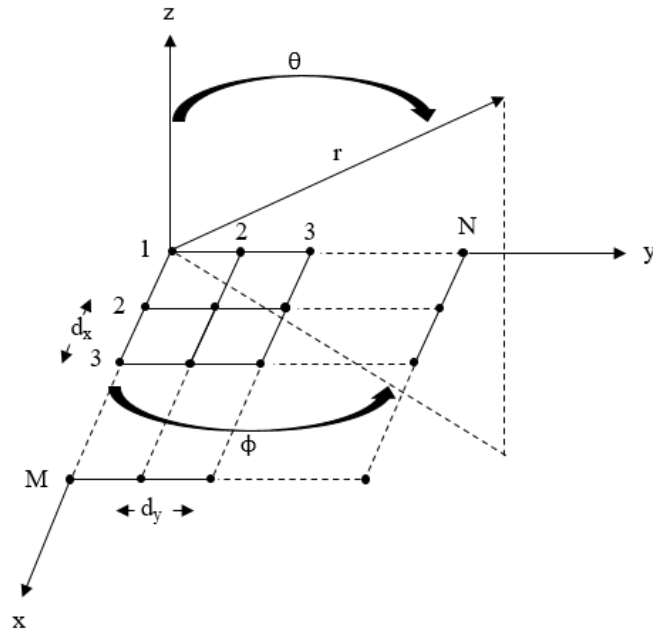


Figure 7. The planar antenna array in the rectangular grid spherical coordinate system. [8]

The array factor (AF) is used for analysing radiation of the antenna array. The geometry of the array and the phase of the signal that is fed to the single antenna is considered forming function for the array factor. When considering identical antennas in the array, any selected antenna in the array multiplied by the AF has the same radiation field as the total radiation field in the far-zone of the array, which leads to the following equation for the planar antenna array:

$$\mathbf{E}(\text{total}) = [\mathbf{E}(\text{single antenna at reference point})] \times [\text{array factor}], \quad (1)$$

where AF is formed considering the number of antennas in a different direction in the array with certain spacing, magnitude and phase. For simplicity, the magnitude of the antenna and spacing is considered to be the same between antennas. The AF can be formed for planar array as follows:

$$AF = I_0 \sum_{m=1}^M e^{j(m-1)(kd_x \sin\theta \cos\phi + \beta_x)} \sum_{n=1}^N e^{j(n-1)(kd_y \sin\theta \cos\phi + \beta_y)}, \quad (2)$$

where I_0 is the excitation coefficient of the array, k the angular wavenumber and β_x and β_y are the progressive phase shift between antennas along the x- and y-axis. [8]

3.6 Massive MIMO

The usage of massive multiple-input multiple-output has become of one the key technology developments for 5G deployment. The first white paper about MIMO was introduced in 1996 by Foschini at Bell Laboratories. [9] It took nearly two decades before it was actually utilized for LTE. The concept of MIMO refers to a wireless system sending multiple different data streams through multiple different antennas to a device utilizing multiple different antennas for reception as illustrated in Figure 7. MIMO specifies at least two antennas used in transmission and reception. The number of streams is always less or equal to the number of antennas. This

same idea is utilized with mMIMO, only the number of antennas is increased to be at least more than 8, which improves spectral efficiency greatly. [1]

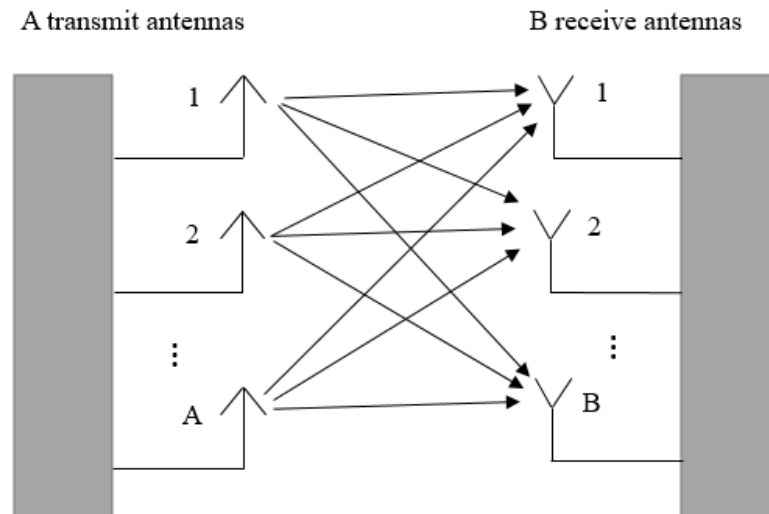


Figure 8. The basic functionality of MIMO.

3.7 Beamforming

The concept of beamforming basically means antenna array radiation pattern manipulation in such a way that it is oriented towards the desired direction vertically or horizontally. This is done analogically, digitally or by combining both with hybrid beamforming. In analog beamforming, the antennas are fed with fixed phase and amplitude at the RF level. The RF signal is adapted with phase shifters, which are relatively cheap to implement, since only one chain is needed in transmission. Digital beamforming is done purely in a digital domain at the baseband, which means that every antenna or array element needs its own TRX chain. It enables the use of multiple beams and MIMO data streams to different directions from a single antenna array. Comparing these two methods leads to combining both, since analog beamforming is cheaper to implement, but has poorer performance than digital beamforming and vice versa for digital. Combining these two forms hybrid beamforming has been attempted to reach performance of digital beamforming, but with lower cost utilizing features from analog beamforming. [10]

4 ANTENNA THEORY

An antenna array is used in the 5G base station to deliver maximum possible data rates with high capacity. While antennas radiate and deliver signal to the user, they also interfere other radiating elements placed next to them in the array. This mechanism is called mutual coupling and it needs to be taken in account while designing antenna array. Strong coupling leads to poor isolation between antennas and can, therefore, decrease the obtainable diversity gains and MIMO capacities in mMIMO systems or even the blocking of another wireless system receiver. [11] This chapter includes the basic theory related to antenna functionality, concentrating on mutual coupling in the antenna array.

4.1 Electromagnetic radiation

Electromagnetic radiation is the law of nature, and James Maxwell modelled it with the following famous equations:

$$\nabla \cdot \mathbf{D} = \rho, \quad (3)$$

$$\nabla \cdot \mathbf{B} = 0, \quad (4)$$

$$\nabla \times \mathbf{E} = -\frac{\partial \mathbf{B}}{\partial t}, \quad (5)$$

$$\nabla \times \mathbf{H} = \mathbf{J} + \frac{\partial \mathbf{D}}{\partial t}, \quad (6)$$

where \mathbf{D} is the electric flux density, ρ the charge density, \mathbf{B} the magnetic flux density, \mathbf{E} the electric field, t the time, \mathbf{H} the magnetic field and \mathbf{J} the current density. From these equations, it can be seen that a magnetic field is created with a changing electric field and the other way around. The possibility for the appearance of self-supporting electromagnetic waves in free space is verified by this. The speed of the oscillation of the electric and magnetic field defines the frequency for radiation and is basic principle to analyse it. Electromagnetic wave has a specific carrier frequency with amplitude and phase. To deliver certain information with it, amplitude and phase can be modulated. This change in time domain changes also the rapidness of the wave and therefore the used bandwidth in the frequency domain. [12]

In the wireless systems, bits are delivered from transmitter to receiver in a radio channel and the number of bits determines how wide a bandwidth is needed. To understand the maximum rate of bits that can be delivered on a single radio channel, the Shannon's capacity formula is formed as follows

$$C = B \log_2 \left(1 + \frac{S}{N} \right) \quad (7)$$

where C is the capacity (bits/s), B the bandwidth and S/N the signal to noise ratio. The limitation of the wireless frequency spectrum is strict since certain wireless signal demands a specific frequency band within a certain area and other systems cannot the same spectrum simultaneously. The crowded state of the modern frequency spectrum requires more efficient spectrum usage and the use of previously unused spectrum. [12]

4.2 Antenna definition

An antenna is defined as an object that radiates electromagnetic waves. However, any object that transfers electromagnetic charge does that. The antenna is determined to be an object that can radiate or receive radio waves travelling in free space. The material of an antenna is commonly metal, but dielectric material can be also used for antennas. In cellular systems, the functionality of the antenna is to transmit and receive radio waves in a certain frequency and with specific bandwidth. This is done by feeding the antenna with electric current and the desired frequency. In Figure 9, the Thevenin equivalent model of a transmission mode antenna is illustrated. There, the antenna is fed an ideal voltage generator V_g with impedance Z_g through the transmission line with impedance Z_T . The equation for the antenna impedance is the following:

$$Z_A = (R_L + R_r) + jX_A, \quad (8)$$

where driven Z_A is the antenna impedance, R_L the loss resistance, R_r the radiation resistance and X_A the radiation reactance. [8] These components comprise the impedance at the antenna port and are divided into the resistive and the imaginary part. The power delivered from the antenna is expressed with radiation resistance and loss resistance is added to it and these comprise resistive part of the antenna impedance. The magnetic and electric near-fields of the antenna are formed partly from the reactive part of the antenna impedance, and the energy is stored to them. [12]

Ideally, energy could be shifted from the source to the radiation resistance R_r without any losses, but actually there are losses due to the mismatches of the antenna and transmission line and the losses of transmission line own nonideal behaviour. In practice, losses can be minimized by designing optimal impedance matching for the system using low-loss transmission lines. Commonly antennas are designed to be reciprocal, which means they are acting same way in transmission and reception. Thus, signals with a certain power delivered from the transmit antenna are received with the receiver antenna in same power, when considering reciprocity. [8]

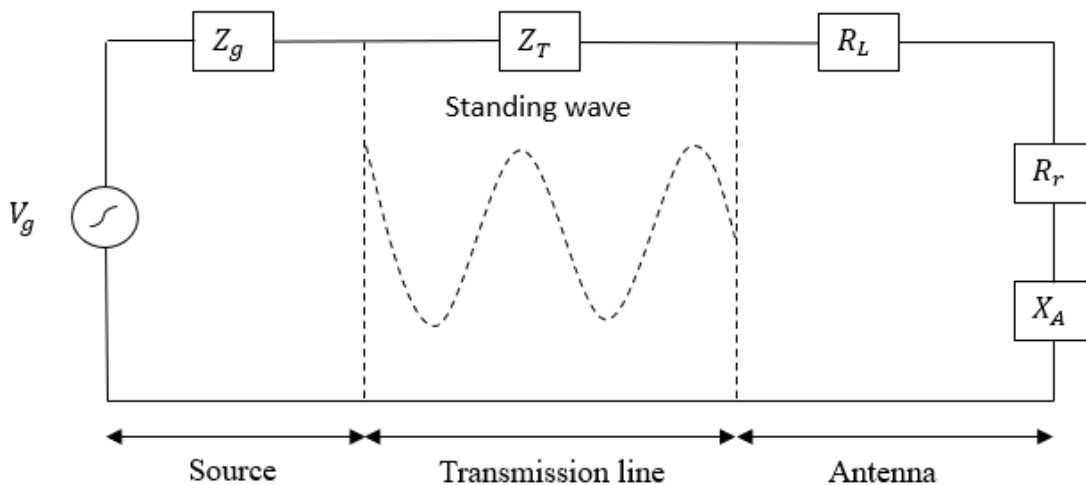


Figure 9. The Thevenin equivalent model of the transmission mode antenna. [8]

4.3 Radiation mechanism

The radiation of an antenna is defined as electromagnetic wave travelling through air. The essential phenomenon behind it can be found from basic physics. When an electric charge moves in a conductor, it generates current. Radiation occurs if the conductor shape is curved, bent or discontinuous. Furthermore, if the electric charge accelerates, decelerates, or oscillates in a time-motion in the conductor, it radiates regardless of conductor shape. So, the antenna is the conductor that is fed by a source, and radiation is generated by a suitable selection of the antenna shape. [8]

4.4 Aspects of propagation

4.4.1 Free-space propagation

While considering isotropic antenna, the electromagnetic radiation happens evenly to every direction as radiated power. The decrease of the power density can be expressed with the following formula:

$$S = \frac{P_t}{4\pi r^2}, \quad (9)$$

where S is the power density towards spherical surface, P_t the transmit power and r the communication link distance. The receiver antenna catches some of the transmitted energy on the receiver depending on the its effective aperture area A_{eff} . The effective aperture area can be expressed with antenna gain as follows:

$$G = \frac{4\pi A_{eff}}{\lambda^2}, \quad (10)$$

where G is the antenna gain, A_{eff} the effective aperture area and λ the wavelength. Describing antenna gain is a direction-dependent measure. It communicates radiation properties to a certain direction compared to cases where the antenna radiates isotopically. However, the transmit and receive power of the wireless system antennas can be described with $P_r = SA_{eff} = \frac{SG_r\lambda^2}{4\pi}$ and $S = \frac{G_t P_t}{4\pi r^2}$. Based on these equations, the Friis's formula is formed as follows:

$$P_r = G_t G_r P_t \left(\frac{\lambda}{4\pi r} \right)^2, \quad (11)$$

where P_r is the receive power, G_t the gain of the transmitter antenna and G_r the receiver antenna gain. [12]

Since the decrease of the received power is relative to $1/r^2$ and with increased frequencies the attenuation of the signal is increased relatively to f^2 , the antenna array is used to achieve higher gain for both transmit and receiver. For the antenna array gain at 0° steering angle the following formula is formed:

$$G_a = 10 \log_{10}(N) + G, \quad (12)$$

where G_a is the array gain, N_e the number of antennas in the array and G the antenna gain. Thus, without the use of antenna arrays the communication link distance would be decreased for 5G systems.

4.4.2 Reflection, diffraction and scattering

When an electromagnetic wave does not reach the user directly from the base station, it can incident into obstacles and reflect, diffract or scatter from it. Reflection happens when an electromagnetic wave conflicts with the planar surface of another material and some of the energy penetrates the material. The coefficient of the reflected and penetrated wave is dependent on angle of conflict, the relative complex permittivity of materials and the polarization of the conflict wave in respect of the surface. While there is an obstacle on in the way of the electromagnetic radiation, diffraction occurs if some of the energy in the wavefront is blocked and it still spreads behind the obstacle on the other way. Now, the result on the other side of the obstacle is a diffracted wave front, which differs from the original. The scattering of the electromagnetic wave happens while it collides with a rough and randomly shaped surface. Scattering occurs evenly into every direction in relation to the standard deviation of the height of the surface depending on the wavelength. It depends on the roughness of the surface if the electromagnetic wave is reflected to orientation of the specular reflection or scattered. The rougher surface is in relation to the wavelength, the more power is scattered. These phenomena can happen also between antennas placed near each other, and this will be discussed later in this chapter. [12]

4.5 Input impedance

The input impedance of an antenna is defined at its pair of terminals. The impedance or voltage to the current ratio at the terminals or the ratio of the appropriate components of the electric to magnetic fields at a point is used to determine the input impedance of the antenna. However, geometry, the excitation method and the location of the ambient objects also affect the input impedance of an antenna. These parameters can be complicated. Basically, the input impedance of the antenna can be calculated by summing up resistances and reactances at the terminals of the antenna. It is reasonable to only analyse simple antennas theoretically, whereas more complex antennas can be analysed experimentally. The reason for analysing antenna input impedance is its importance for antenna matching. In practice, the antenna is fed by a feedline, which needs to be matched to the antenna input impedance to minimize the reflections and radiation losses of the antenna due to mismatching. Since the input impedance of the antenna is changing in terms of frequency, the desired antenna bandwidth is taken into account in antenna matching. [8]

4.6 Radiation pattern

An antenna radiation pattern is a way to illustrate antenna radiation characteristics as a function of space coordinates. Usually, it is analysed in the far-field, which is the furthest antenna radiation region from the antenna where the actual user is in practice. Radiation characteristics consist of the power flux density, radiation intensity, field strength, directivity, phase or polarization. Commonly, the spatial distribution of the radiated energy as a function of the observer's position along a path or surface of the constant radius is under surveillance in the two- or three-dimensional coordinate system as illustrated in Figure 10. The radiation pattern of the base station antenna is designed to be directional, where there are one major lobe and undesired minor lobes. Thanks to this, the antenna radiation is the most powerful in a certain direction. The base station antenna radiation is usually observed by measuring the antenna gain or directivity in decibels (dB) in the two-dimensional coordinate system, where the azimuth or elevation angle is set to a certain angle and the other is changing 360° . [8]

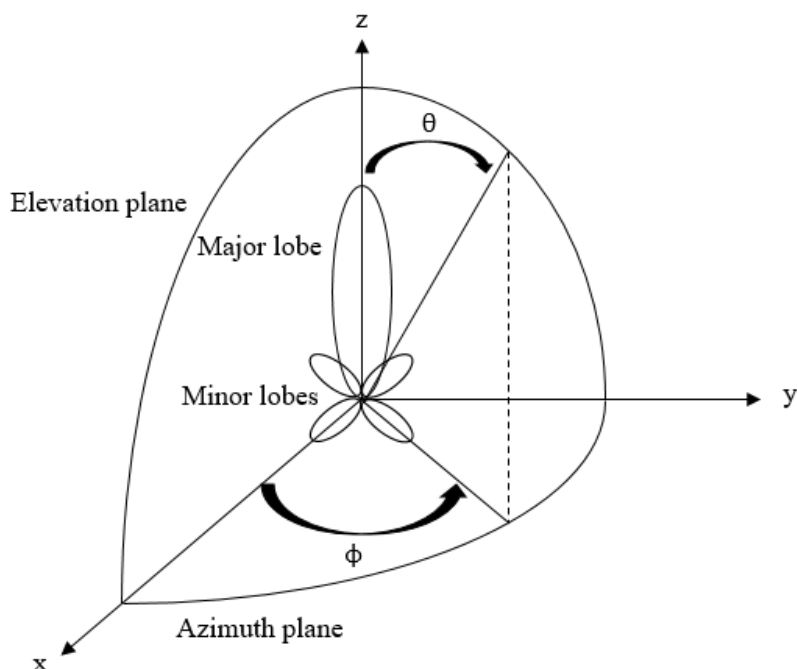


Figure 10. Radiation pattern in the three-dimensional coordinate system. [8]

4.7 Scattering parameters

To use an antenna properly, it needs to be connected to a transmitter, a receiver or a transceiver. The transmitter feeds information signals to the antenna and receiver catches this signal from air. The transceiver can do these both and is used in base stations. Ideally, the power transmitted from the transmitter would be the same in receiver, but the impedance matching of these components to the antennas affects how much power is delivered. The ratio of the voltage and the current determines this impedance at the antenna port. It is complex and contains a real resistive and an imaginary reactive component. To analyse the antenna array with multiple ports, scattering parameters (S-parameters) are used to characterize them. The following equation for network of two ports is formed:

$$S_{ij} = \frac{V_i^-}{V_j^+}, \quad (13)$$

where S_{ij} represents port which is measured, V_j^+ is the voltage which is fed only to the port j and V_i^- is coming from the port i as a reflected wave and its amplitude is measured. [12] While considering the antenna array system consisting of two antennas, the reflection coefficient S_{11} is used to determine the signal resonant frequency and the bandwidth passed to the antenna from port 1. The isolation between the antenna array ports is measured between port 1 and 2 with S_{12} . So, the antenna's resonant frequency, operation bandwidth and isolation between ports can be determined. In antenna arrays, there are multiple antennas, and every antenna needs to be fed separately to observe scattering parameters of them.

In practice, the analysis of the antenna isolation between certain ports has to be done by also taking into account the antenna reflection coefficients of those antenna ports. It is because "the S_{ij} describes the ratio of the incident voltage wave on port j to the output i and not the ratio with the actual accepted voltage wave at port j " [12]. Therefore, if power is not delivered high enough on a certain frequency to one port, it will increase its isolation to another port. This is not appropriate since antenna matching needs to be at least -10 dB for a single antenna to reach the desired radiation performance for the antenna.

4.8 Mutual coupling

Antenna mutual coupling is an undesired phenomenon, where at least two separate antennas are close to each other and some of the radiated energy is radiated towards each other. It can be measured with the S-parameter S_{ij} , if $i \neq j$. Isolation between antennas is the inverse of the mutual coupling and it is a commonly used quantity while dealing a multi-antenna system. [11] All antenna radiation properties, distance and direction related to each other, affect how much energy is radiated between the antennas. Mutual coupling can occur in both transmission and reception in many ways. However, they have to be analysed individually. [8]

To describe phenomenon theoretically, the following equations are made to create empirical model of the mutual coupling:

$$\begin{aligned} C_{ij} &= \exp\left(-\frac{2d_{ij}}{\lambda}(\alpha + j\pi)\right), \quad i \neq j \\ C_{jj} &= 1 - \frac{1}{N} \sum_j \sum_{i \neq j} C_{ij}, \end{aligned} \quad (14)$$

where C_{ij} is the mutual coupling, d_{ij} the distance between the i th and j th antennas, accordingly, and α is the parameter used for coupling level characterization. Nonetheless, the excitations of the other antennas and array geometric configuration matter regarding individual antenna mutual coupling. In practice, the mutual coupling between the i th and j th antenna is defined with a dB-valued S-parameter called isolation, $-20\log_{10}(|S_{ij}|)$. [13]

4.8.1 Transmission mode

In transmission, energy radiated from one antenna can be received partly by another antenna close to it and some of the energy can be rescattered to other directions and even back to the

original antenna. While an antenna absorbs undesired waves due to mutual coupling, it will change its standing wave pattern. The coupled wave and reflected wave differ from each other only in amplitude and phase while considering coherent excitations. Their interaction is related to the coupling between them and their excitation. The sum of these vectors is equal to the influence of the input impedance of the antenna terminals and it varies proportionally depending on the position and the excitation of the antenna that caused the mutual coupling. This change in certain antenna driving impedance is commonly referred to as mutual impedance variation. [8]

The illustration of the mutual coupling effect in transmitting mode is shown in Figure 11 with two antennas m and n in an array. A source connected to element n is generating a signal through the transmission line into element n (as arrow 1. shows). Element n radiates this signal to space (2) and towards element m (3). Element m receives most of the signal's energy (5), and a portion of the energy is rescattered towards space (4) and element n (6). This rescattering between elements can happen repeatedly until the energy is reduced to negligible. [13]

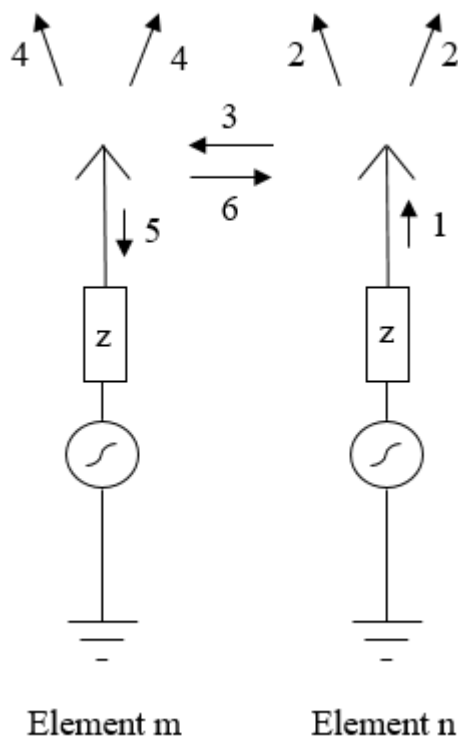


Figure 11. Mutual coupling in transmit mode. [13]

4.8.2 Reception mode

While the base station is in reception mode, mutual coupling occurs as follows: A certain antenna receives energy and rescatters some of the energy to any direction and towards antennas placed near it. For the receiver antenna, the accuracy of the antenna matching to terminating impedance affects how much energy is received and rescattered. Obviously, antenna matching should be done as well as possible to minimize mutual coupling in reception. Since the coupling paths and the excitations of the transmitting and receiving antennas are unequal, they cannot be considered to be the same. [8]

In Figure 12, mutual coupling is illustrated in reception mode with two antennas m and n . Incident wave front travelling through space arrives to elements m and n (1). Due to the slanted orientation of the wave front compared the antennas, it first arrives to element m before n . Most of the energy is received by antenna m (2) and a part of the energy is added vectorially to the incident wave (5). The rest of the energy is rescattered towards space (3) and element n (4).

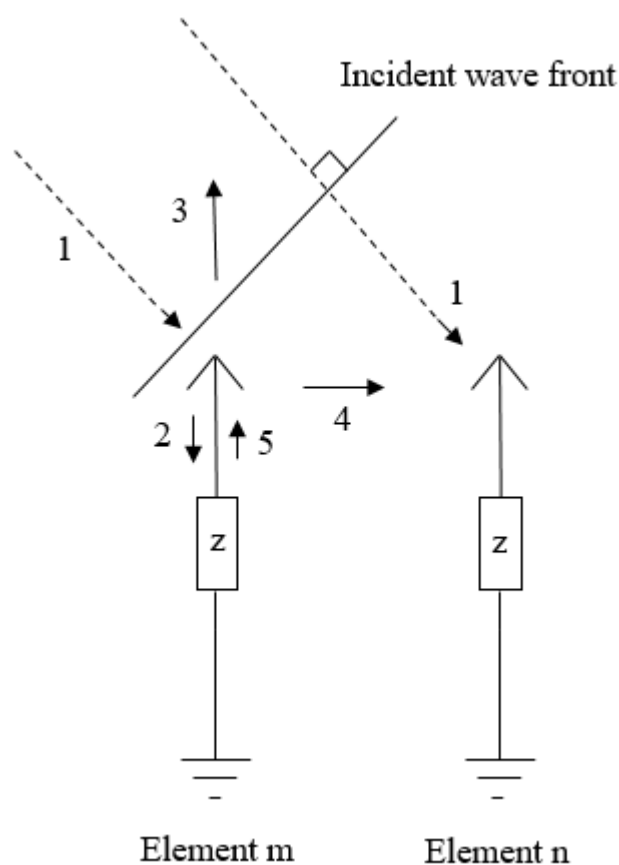


Figure 12. Mutual coupling in reception mode. [13]

4.9 Driving impedance

The excitations of other antennas affect the impedance of individual elements in the antenna array. The weight of the impact to a single antenna can be divided based on the excitation of the surrounding antennas. If the antenna is surrounded by passively terminated antennas, it is called passive driving impedance. On the other hand, active driving impedance means that a single antenna is surrounded by excited elements. Even though these do not differ from each other much, the term “driving impedance” is used commonly to consider active driving impedance. For a single element in the antenna array, the driving impedance depends on the placement and excitation of the other elements. So, for different antenna array elements the optimum input impedance varies for different excitations, which maximize the array gain. [8]

4.10 Mutual coupling in the array microstrip antennas

For the antenna array, mutual coupling affects every antenna in the array in an individual way changing the antenna manifold, input impedance and radiation pattern. How much it is affected depends on the antenna type and its design parameters, antenna spacing in the array, the feed of the antennas, antenna distance from the ground plane and the scan volume of the array. Furthermore, if the antenna is above the ground plane the ground plane shape and dimensions affect the coupling since it acts as a reflector reflecting radiation from the antennas towards the ground plane. Coupling between antennas is considered direct coupling and any structures between the antennas can cause incident coupling to the antennas. The usage of dual polarized antenna leads to the internal coupling of the antenna. This coupling occurs through the surface and in the air in both transmission and reception, and attempts are made to minimize it with a suitable phase difference of the antenna feeding. Due to mutual coupling, the corner and edge antennas of the array are affected by different driving impedance and the impact of mutual coupling is lower. Therefore, antenna mutual coupling strongly affects antenna array performance and the methods to minimize it need to be chosen wisely.

4.11 Cross polar discrimination

The usage of the dual polarized antenna in the base station improves the overall system performance with polarization diversity gain. However, different polarizations need to be isolated from each other. Cross polar discrimination (CPD) means how well each polarization can transmit or receive its own polarization and reject the transmission or reception of different polarization. It is measured by taking the magnitude of the relative power of the main polarization pattern and making it proportional to the cross polarization pattern at a certain angle. It is commonly investigated in the form of two-dimensional radiation pattern in a certain radiation sector or angle. In the Figure 13, an example of the rectangular plot of the realized gain on the azimuth cut is illustrated. There, the elevation angle is set to 0° and the realized gain is plotted from -180° to 179° azimuth angle. Here, the realized gain for co and cross polarizations can be seen, and cross polar discrimination is simply the difference between of these two. [14]

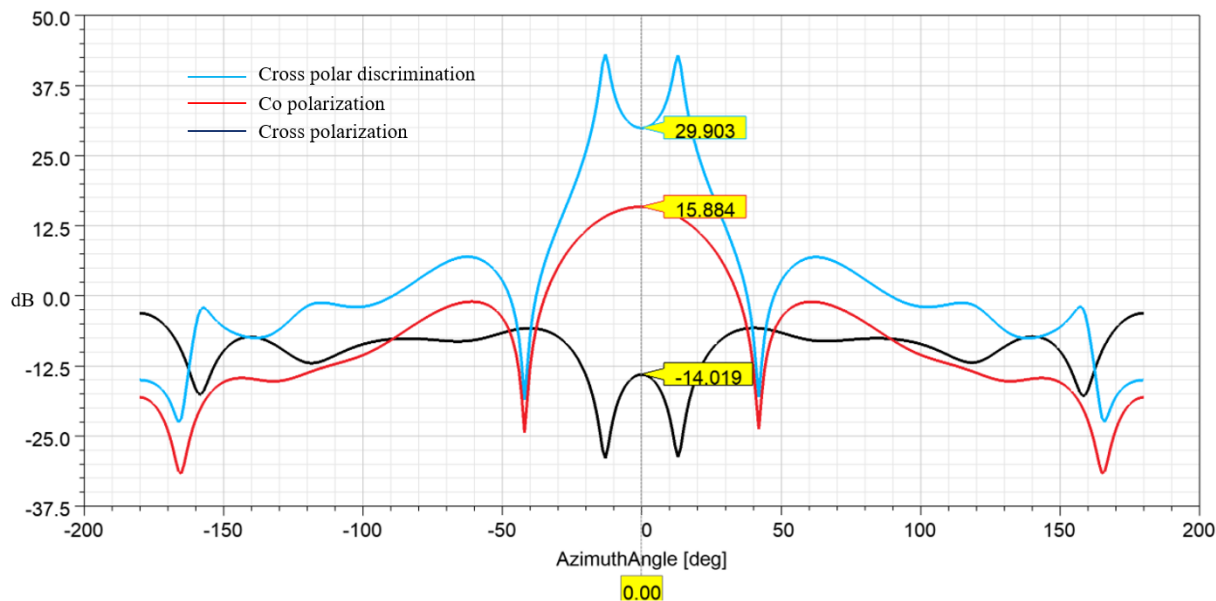


Figure 13. The rectangular plot of the realized gain on the azimuth cut while elevation angle set to 0° .

4.12 Decoupling techniques in antenna arrays

Mutual coupling has been a well-known phenomenon for researchers and the wireless industry for a long time and there is a large number of studies related to it. Isolation between the antenna ports is very important for the performance of mMIMO and the phased array, since communication capacity, beamforming and linearity of PA require it to be low enough. In literature, many methods have been covered to utilize decoupling for the base station antenna array. For example, “electromagnetic bandgap structure, LC-based network, distributed circuit-based scheme, decoupling meta surface, defected ground and scatter-loaded scheme” are possible methods for decoupling. [15] These structures were applied in a small antenna array and designed to optimize only a few design parameters. To actually use them in practice, the improvement of isolation between ports cannot be done without detriment to other design parameters. Thus, good radiation performance, compact size, low cost and weight need to be maintained.

The antenna type and placement on the ground plane determine how radiation occurs towards the user and other antennas producing mutual coupling between antennas. The isolation method to prevent coupling must be chosen and designed based on these design parameters. In this work, the microstrip patch antenna is used and since it is air filled from ground, also isolator elements must be above the ground plane. This reduces the amount of available research material since most of the research does not utilize the same kind of air filled from ground antenna structure as in this work. In the initial antenna array design of this work, the isolation elements were placed between the antenna to improve isolation between ports. These isolation elements act as wave trap elements and can be metallic walls or posts optimally placed between antennas. With these implementations, the highest isolation of -18.57 dB between ports has been achieved, and in this thesis the main aim is to try to improve to it to -30 dB.

5 OBSERVATION OF ANTENNA MUTUAL COUPLING

In this chapter, the initial antenna array design and the root causes for antenna coupling are studied. The goal for this thesis is to improve port-to-port isolation to be at least -30 dB from any port to any other port. This needs to be done while maintaining the main radiation performance properties of an antenna array. The S-parameters and radiation pattern results for the initial design are used as main reference parameters to compare the performance of the proposed methods to improve isolation. Electromagnetic design and simulation tool Ansys HFSS are used for the simulations as the effective tool for the large symmetrical antenna array simulations.

5.1 Initial antenna array design

The initial state of the design is the antenna array model of Nokia, which is already in the deployment phase in the field. This antenna array is designed to operate in the 3.3–3.8 GHz band using dual polarized patch antennas. The antenna array is configured with three patch antenna elements placed parallel to each other as a sub array. These three antennas are fed to different polarizations with individual feedlines from their own port as illustrated in Figure 14. The sub arrays are configured to full antenna array with 8 columns and 12 rows. Every sub array is fed through two ports so that different polarizations are fed from individual ports. Overall, there are 32 sub arrays, with each of them having two individual linear cross polarizations. Each polarization of the sub array has its port, so the full array has 64 ports in total. The individual TRX branch is connected to every port, making an overall 64 TRX chains in the base station.

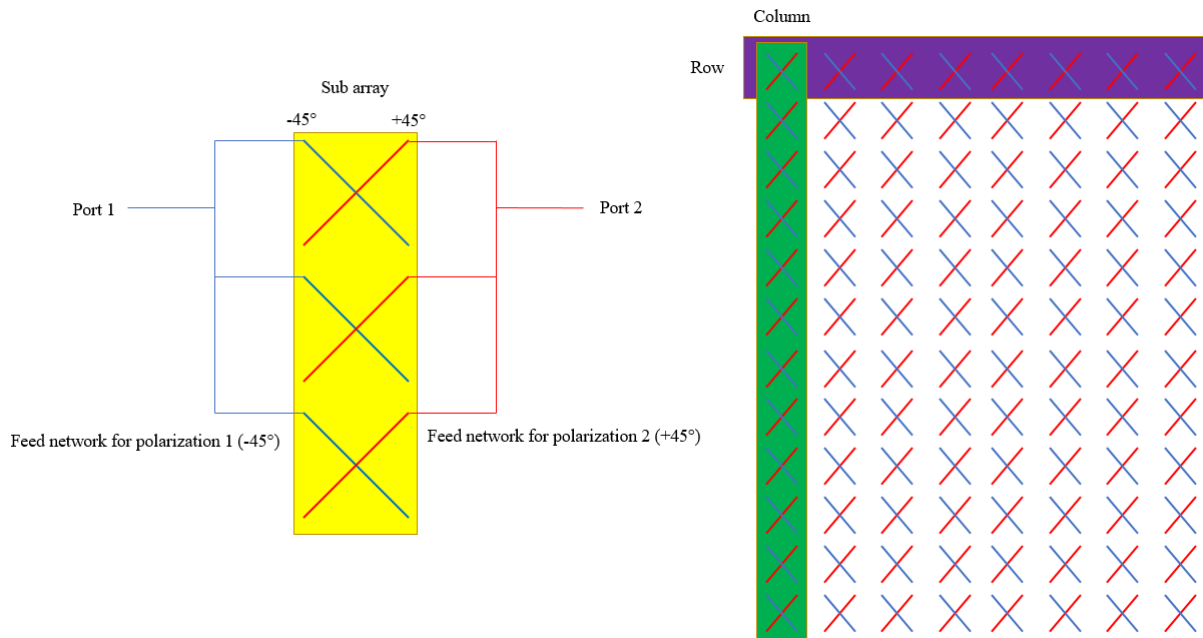


Figure 14. Antenna sub array and full array configuration.

5.1.1 Air insulated dual polarized balanced probe feed microstrip antenna

Polarization diversity enables the base station to transmit and receive electromagnetic waves in two different polarizations. This is done with an antenna structure called “air-insulated dual-polarized balanced probe feed microstrip antenna” as illustrated in Figure 15. There are two linear $\pm 45^\circ$ slanted cross polarizations, which are fed from two different probes. The high isolation between polarizations is met with feeding each polarization with signals that have equal magnitude, but a 180° phase difference between antenna “legs”. This is done by designing the feed network to the patch way as shown in Figure 16. The different length of the feedlines means that the phase difference between leg 11 and 12 as well as leg 21 and 22 are equal to 180° . With this method, the coupling between leg 11 and leg 22 is invalidated by the coupling between leg 12 and leg 21. [15]

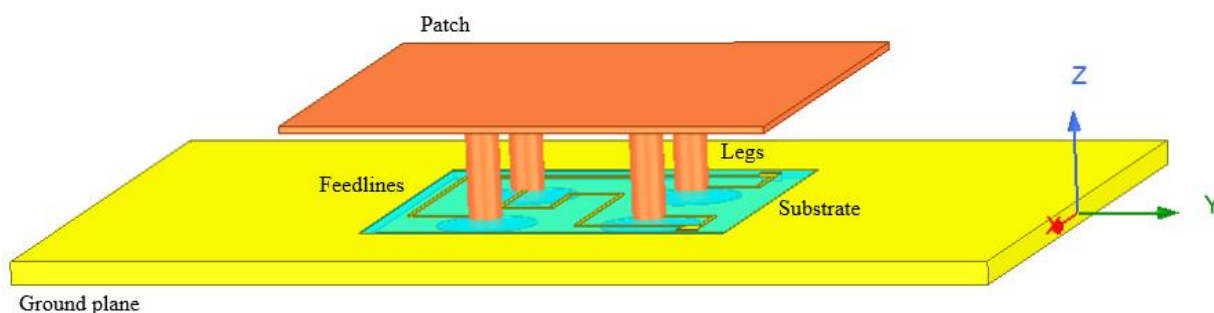


Figure 15. Air insulated dual polarized probe feed microstrip antenna.

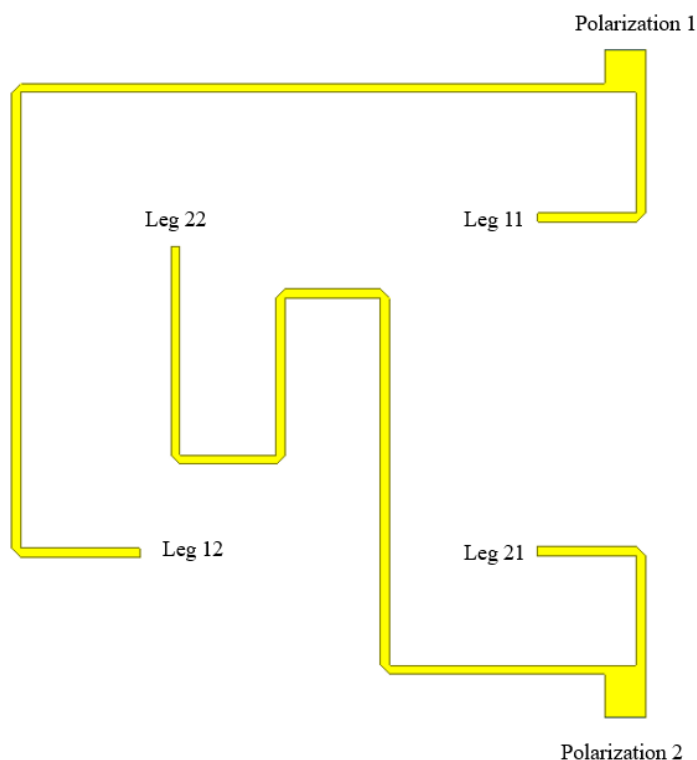


Figure 16. Feedlines to the "legs" of the patch.

5.1.2 Antenna array design

The antenna design and simulations are performed using Ansys HFSS. The layout of an individual sub array is presented in Figure 17. There are three antennas and feedlines placed top of printed circuit board (PCB). The isolator elements are placed around each antenna element to provide isolation between the antennas and the cross polarizations, which also affect antenna matching. A radome is located to above the antennas, and it is very important to have one in simulations since it affects the performance of the array radiation pattern significantly. The feedline for the sub array is shown in Figure 18. There it can be seen how each antenna has a different length feedline. It provides a phase difference of 26.3° between elements 1 and 2 as well as between 2 and 3. This way the -6° vertical pretilt is achieved for the radiation pattern of the individual sub array and the whole antenna array.

Ansys

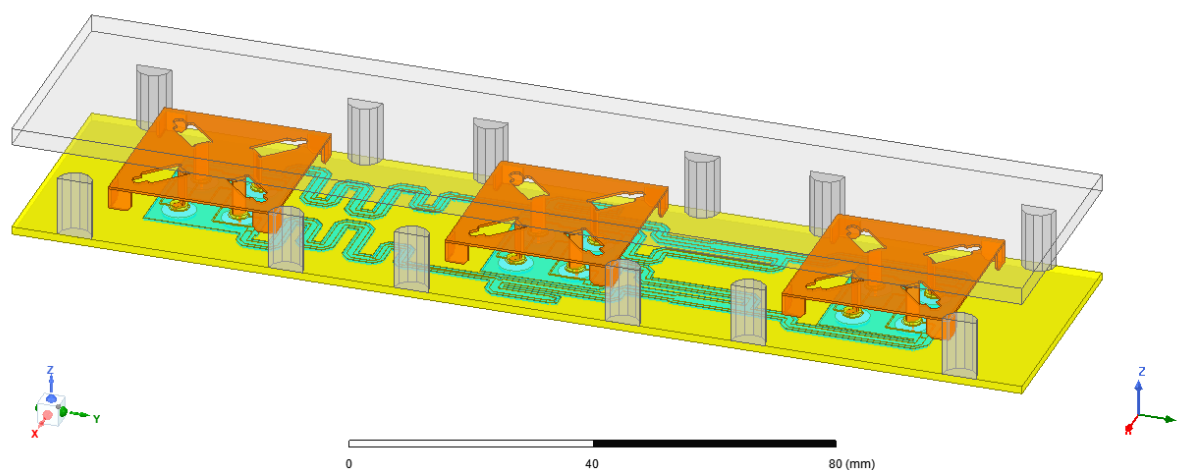


Figure 17. Antenna sub array for the initial design.

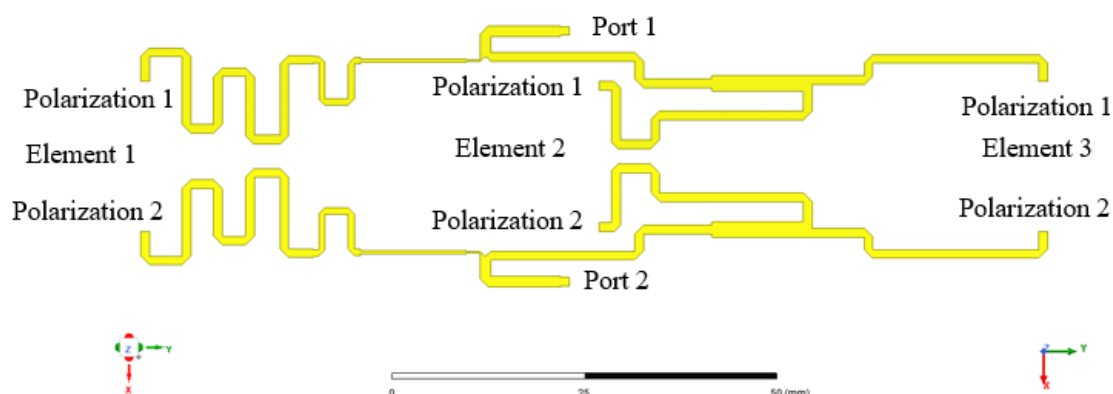


Figure 18. Feed network for the sub array.

The 3D layout of the full antenna array is formed using a 3D component of the antenna sub array. These 3D components are placed as in full array configuration. An advantage of the Ansys HFSS simulation software is the fact that it speeds up the EM simulation for the big symmetrical structure. The S-parameters and radiation pattern of each 3D-component are calculated on their own and the full array radiation pattern is formed based on those results. The initial full antenna array design is shown in Figure 19. In practice, the antenna array is placed in the base station so that its y-direction is pointing towards the atmosphere and the antenna radiation towards z-direction where actual users are.

Ansys

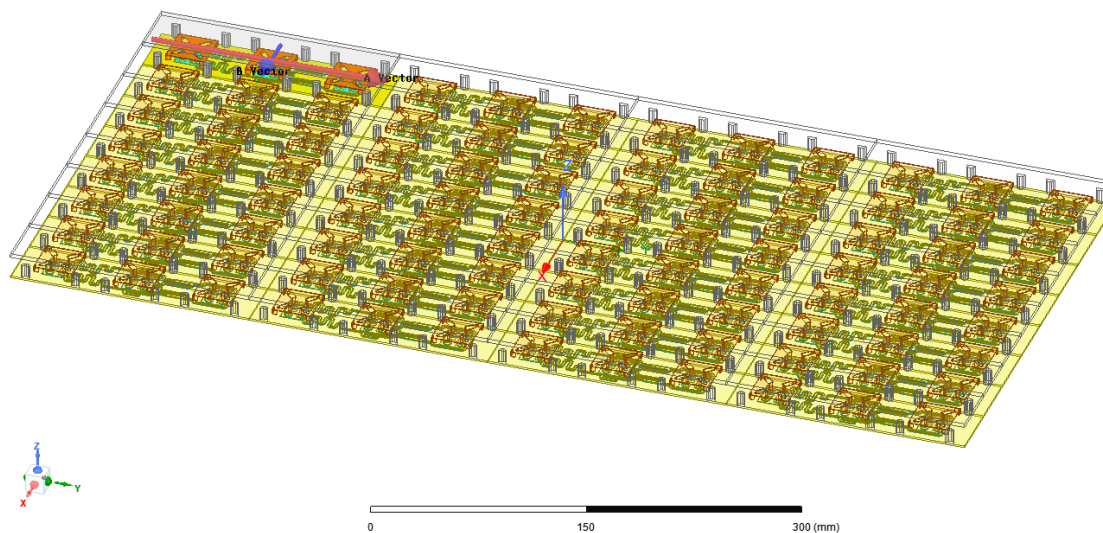


Figure 19. Initial full antenna array design.

5.1.3 Initial results for antenna matching and port-to-port isolation

An initial antenna array design is illustrated in Figure 19. The whole array includes 64 ports and it is not reasonable to illustrate the matching and port-to-port for every single sub array individually. The antenna matching for an individual port should be -14 dB, and the worst-case scenario for port-to-port isolation is shown in Figure 20. There, the internal isolation of the sub-array [1,1] is -18.74 dB. This internal coupling of sub-arrays restricts the isolation for the initial design. In the Figures 21 and 22, the internal coupling of sub-arrays located in the first and eighth column are illustrated. There it can be seen how the higher in the column sub-array is located, the better isolation gets. These sub arrays located in the sides of the array are the worst in terms of internal isolation compared to sub arrays located in the middle of the array. Regarding other isolation factors, the results were about -20 dB or better and these will not be shown in this thesis to save space. As the simulation of this full array takes a comparatively long time, a simplified version in the Figure 23 is used to save simulation time and computer memory since only four horizontally side by side placed sub arrays are used with surrounding “empty” cells, which contain only the radome and the ground plane. The two sub arrays [3,4] and [3,5] are analysed and their impedance matching is shown in Figure 24, whereas the internal isolation and port-to-port isolation between these sub arrays are in Figure 25. There, the internal isolation of both sub arrays, -20.97 dB, can be seen. It is the main restricting factor for this kind of simulation model.

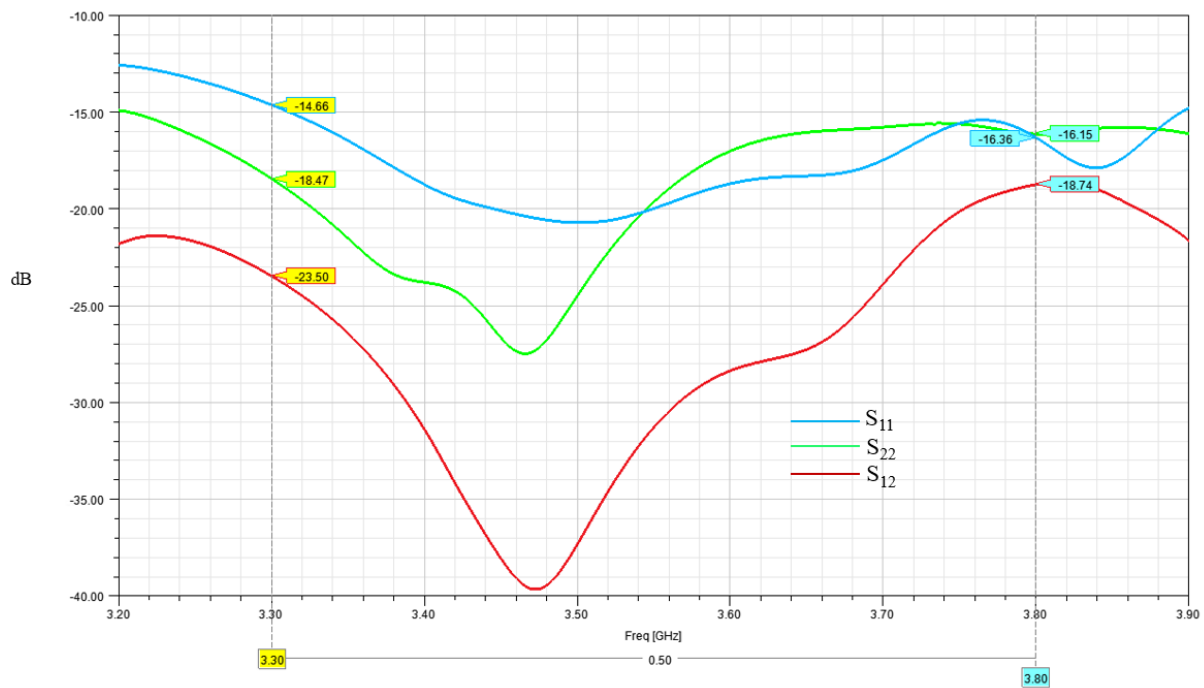


Figure 20. The S-parameters of sub-array [1,1].

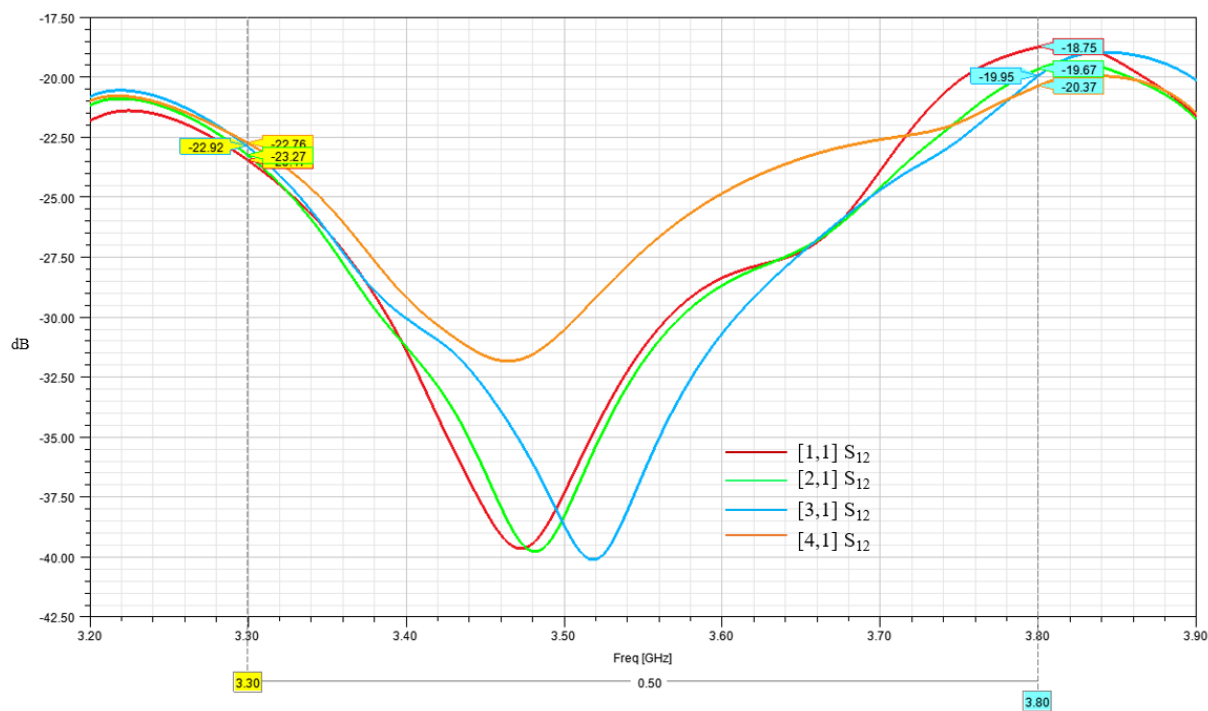


Figure 21. The internal coupling of the sub-arrays located in the first column.

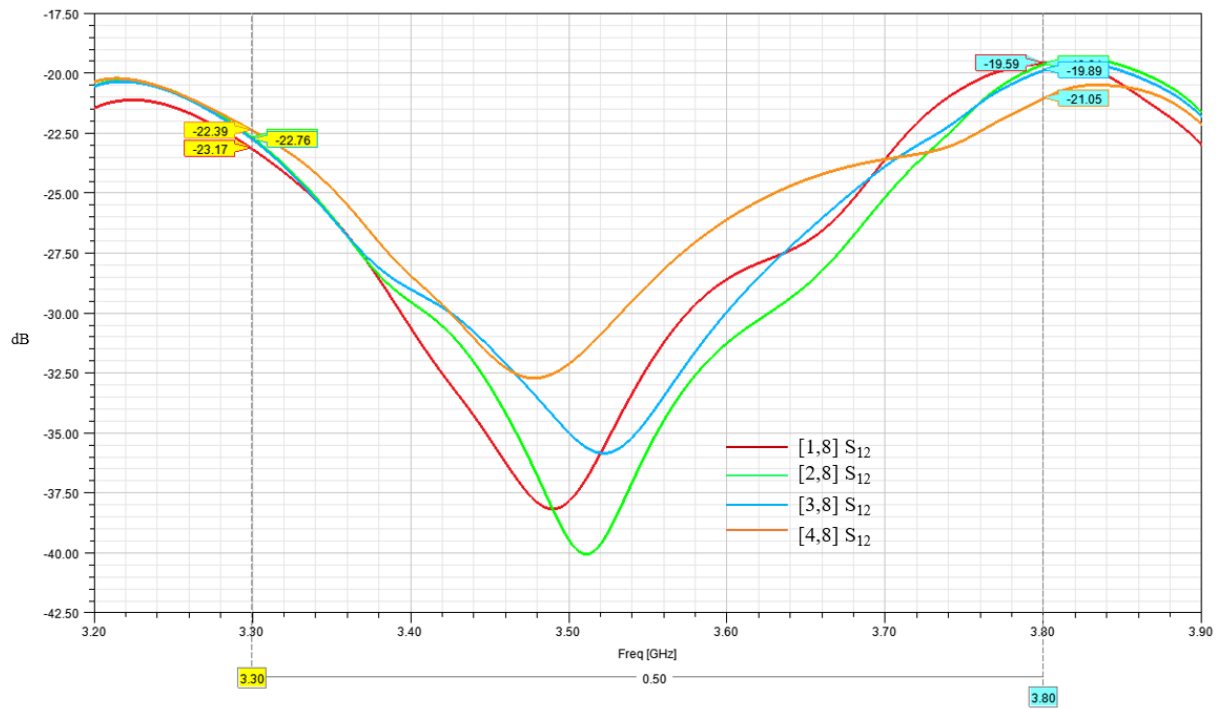


Figure 22. The internal coupling of the sub-arrays located in the eighth column.

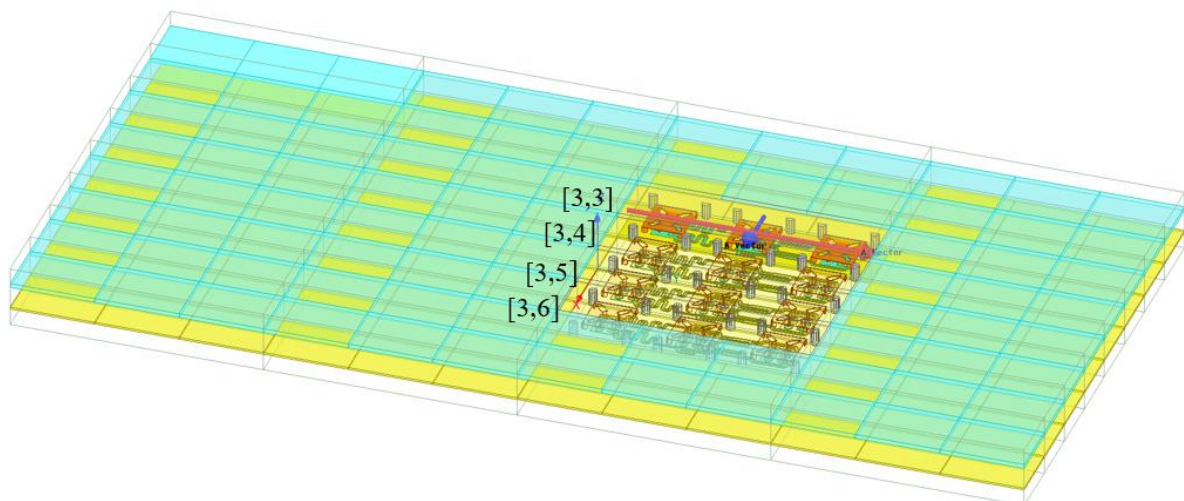


Figure 23. The simplified simulation model for sub array with a fast simulation time.

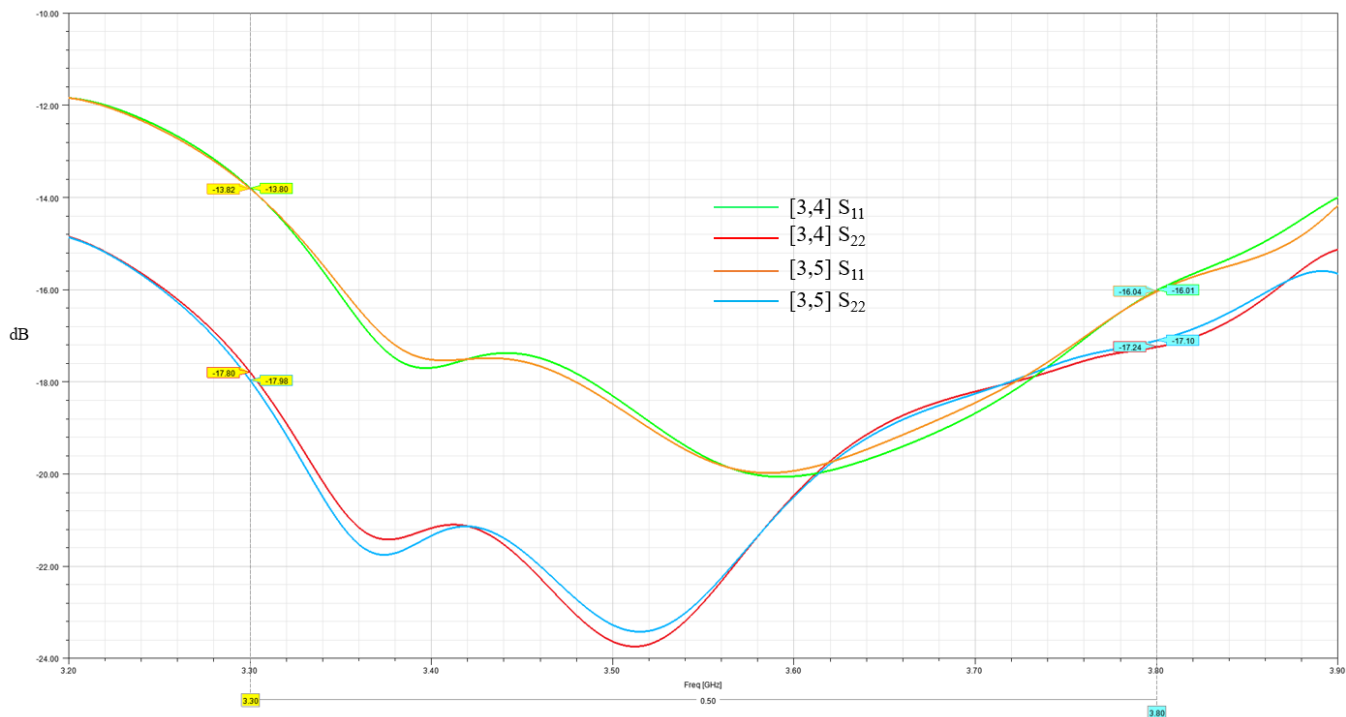


Figure 24. The impedance matching of sub arrays [3,4] and [3,5].

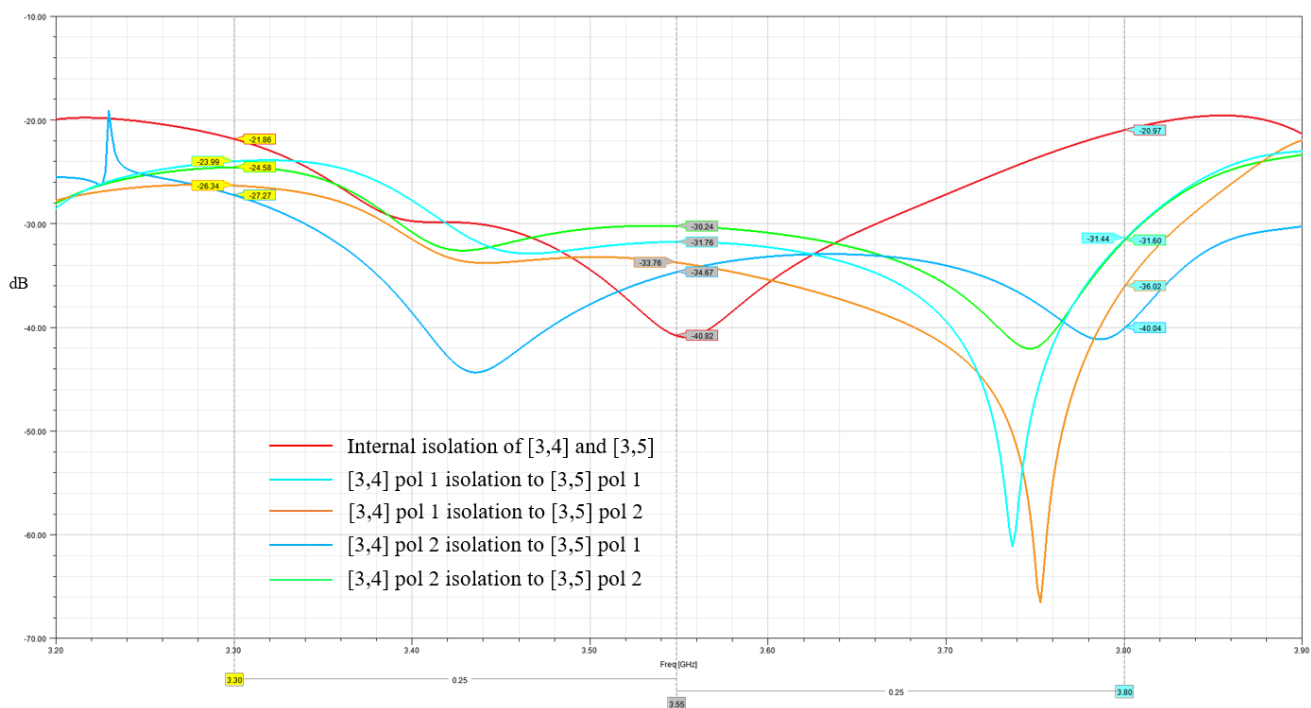


Figure 25. The internal isolation of sub arrays [3,4] and [3,5] and isolation between sub arrays [3,4] and [3,5].

5.2 Root causes of implementation for antenna coupling

In the initial state of the antenna design, there are isolators providing isolation between antenna feeding ports. These isolator elements act like wave trapping elements, blocking signal

travelling between sub arrays. Furthermore, these isolator elements provide antenna matching and affect the overall radiation pattern of the antenna array. So, if the isolator elements would be removed from design, the antenna would not be matched well for the operation bandwidth, and the isolation between the antenna ports would not be low enough. This happens because any structure around the antennas changes the antenna manifold, input impedance and radiation pattern. The isolation of dual-polarized antennas can be split between the internal coupling of an individual antenna and the mutual coupling of two or more antennas. The S-parameters are used to define isolation between ports, and a useful way to illustrate how radiation occurs between polarizations and antennas is to animate electric and magnetic fields in the structure. In this section, it is done to identify the factors restricting isolation performance without the isolator elements.

5.2.1 Antenna mutual coupling in small array

The phenomenon of mutual coupling is simulated next in the small array, as shown in Figure 26. There are three by three arrays where all antennas are active. The isolator elements are removed from this simulation to observe the isolation from the middle element [2,2] to surrounding elements. In Figure 27, it can be seen how the antenna matching is shifted upwards to 290 MHz, due to the removal of the isolators. Therefore, it is reasonable to also observe the isolation on the correct band since matching affects isolation drastically.

In Figures 28 and 29, the isolation of the antenna [2,2] to antennas [2,1] and [2,3] are shown. There can be seen how the isolation between the same polarizations have the worst isolation on lower corner frequency and on higher corner frequency isolations between different polarization are almost as bad. In this simulation, the internal isolation of [2,2] does not restrict the isolation as much as coupling between antennas. The isolation of other antennas which were better than -20 dB are not shown here to save space.

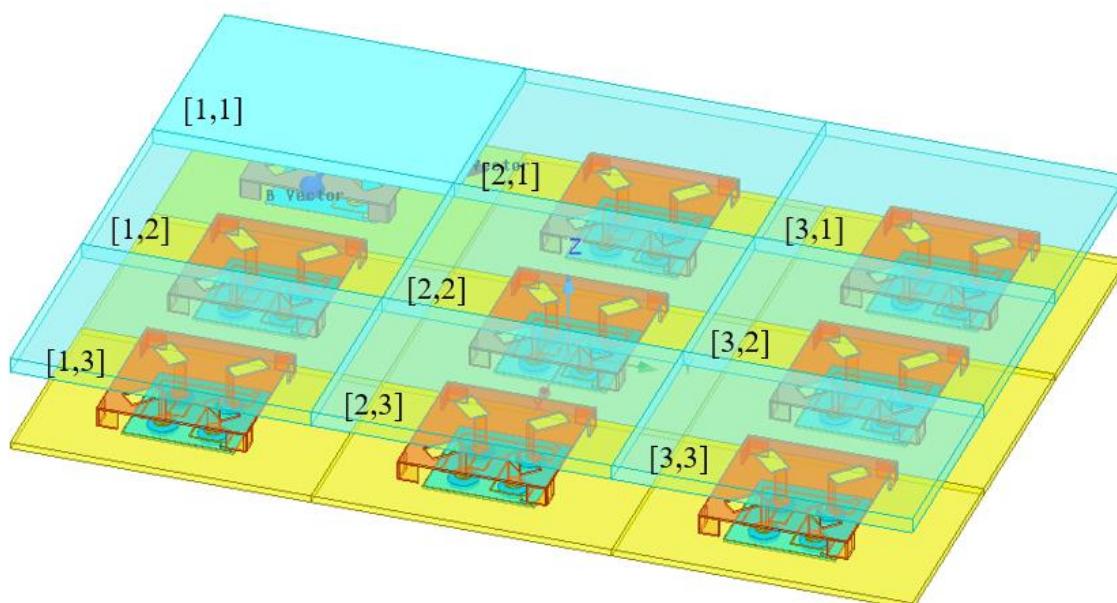


Figure 26. The simulation model to illustrate mutual coupling in a small antenna array.

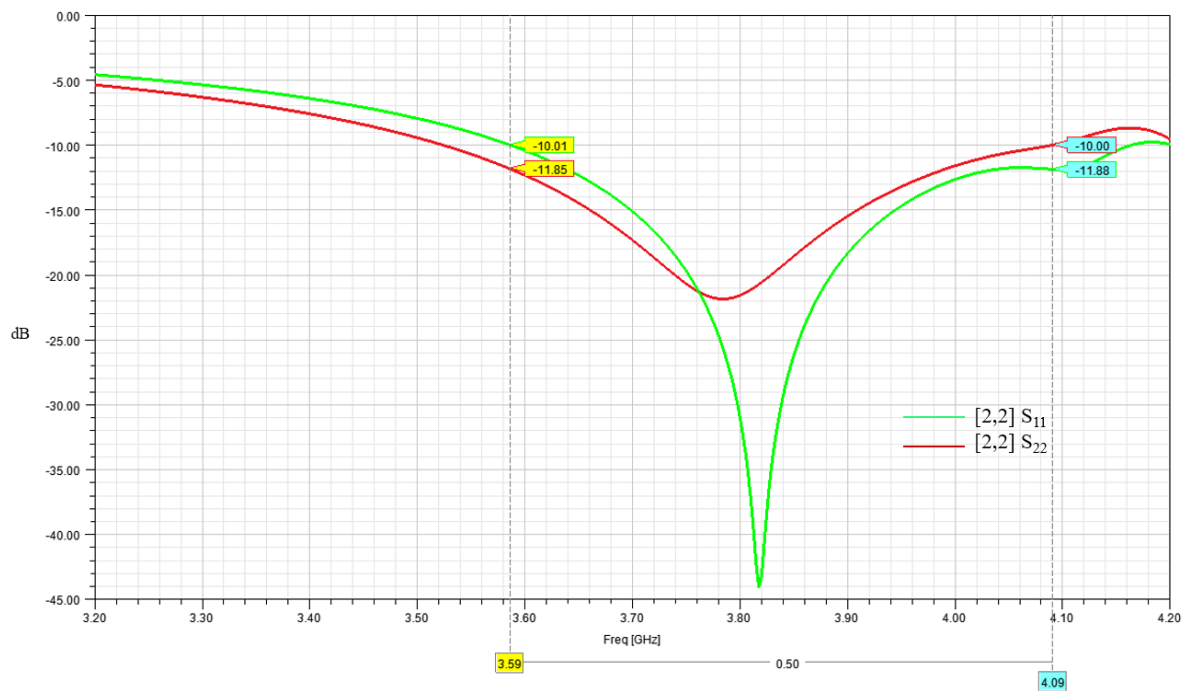


Figure 27. The impedance matching of antenna [2,2].

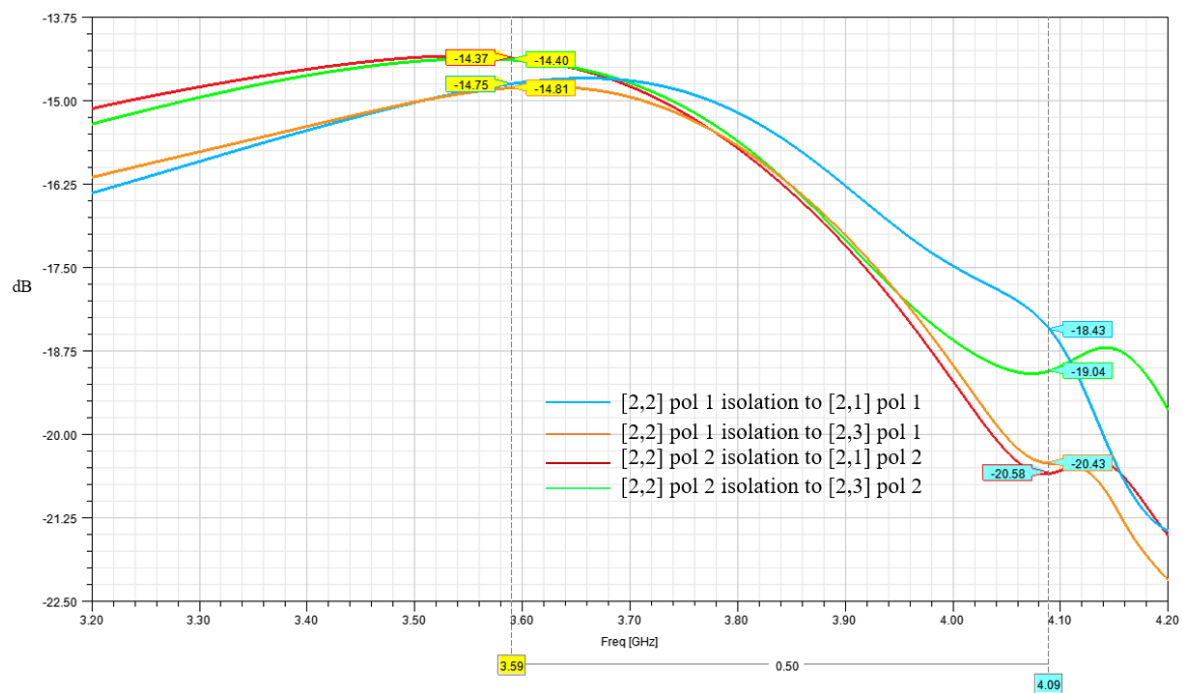


Figure 28. The isolation of antenna [2,2] to antennas [2,1] and [2,3] considering the same polarization.

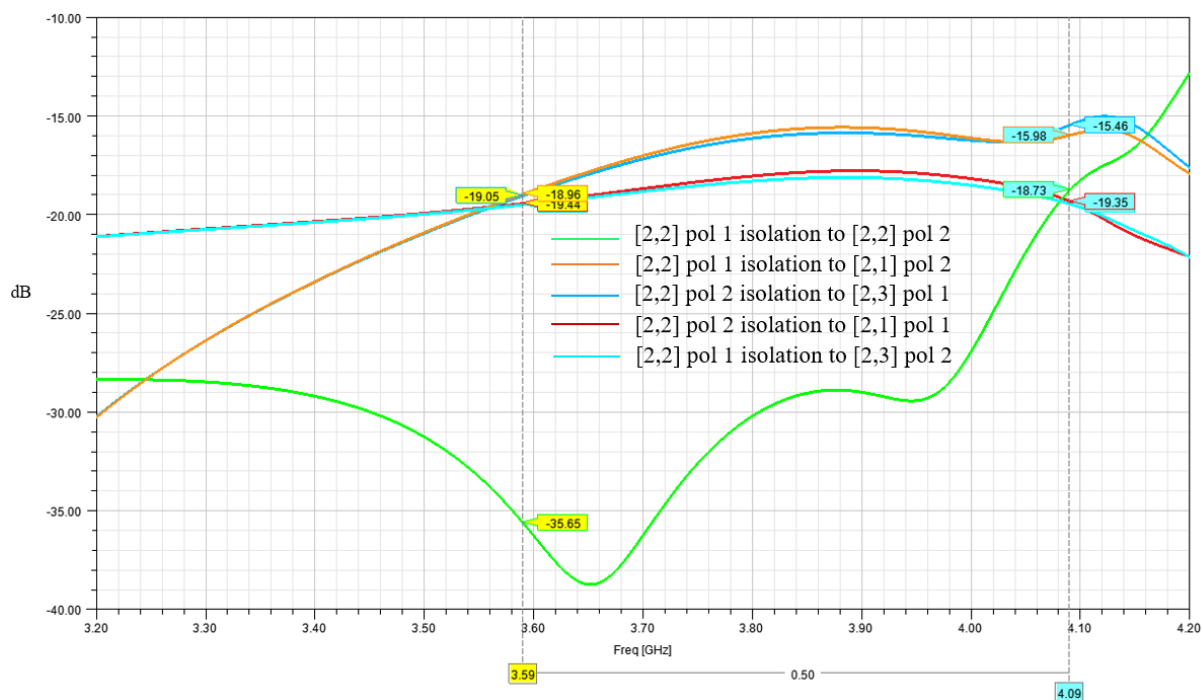


Figure 29. The internal isolation of antenna [2,2] and the isolation of antenna [2,2] to antennas [2,1] and [2,3] considering different polarizations.

5.2.2 Behaviour of electromagnetic fields in small array

It is possible to animate electromagnetic fields to a certain surface in the design with Ansys HFSS. The same three-by-three antenna array is analysed as in the last section. The behaviour of the electric field is animated from phase 0 to 360 degrees at 3.84 GHz. This 3.84 GHz is chosen since without isolator elements the antenna resonant frequency is shifted upwards by 290 MHz. The usage of the actual centre of the resonant frequency should give reasonable information about how radiation occurs from antenna to another. In Figures 30 and 31, the electric field (E-field) distribution is animated at the planar surface on top of the antenna array at 3.84 GHz. Only the middle antenna element is active and rest of the antennas are passive. Two the most essential phases of radiation are chosen for these Figures from each polarization. The differences in the electric field distribution can be seen while simulating each polarization like those used in actual base stations. In these Figures, it is seen how coupling occurs to the surrounding elements. The coupling is the highest to horizontal elements, then to the vertical and the lowest to corner elements, as simulated in the last section.

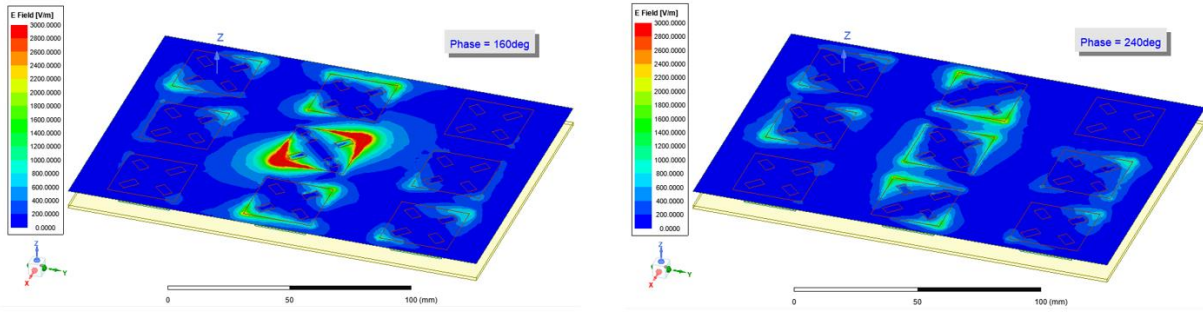


Figure 30. The distribution of E-field on planar surface at the top of antennas in the small antenna array is presented at 3.84 GHz with only polarization 1 of middle antenna active.

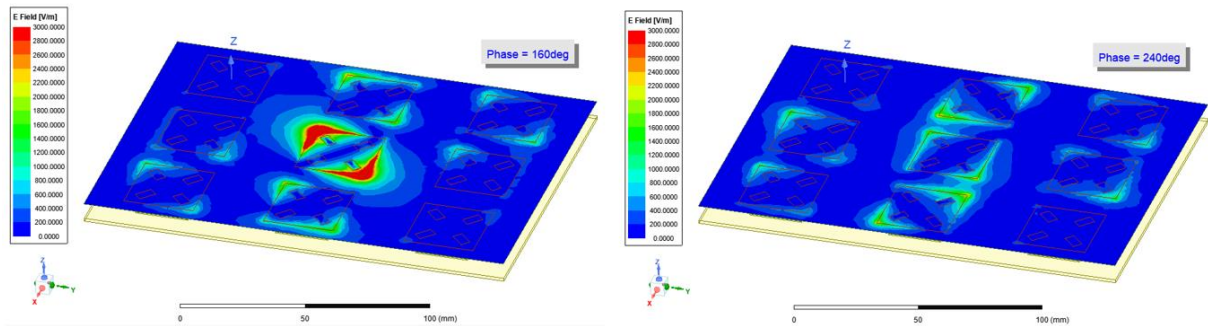


Figure 31. The distribution of E-field in the small antenna array at 3.84 GHz with only the polarization 2 of middle antenna active.

5.2.3 Impact of phased feed network

The individual sub array is fed with a phased network to provide a -6° pre tilt on the radiation pattern elevation angle. This affects the coupling between antennas and is illustrated in this section without the isolator elements. The simulation model to observe that effect is shown in Figure 32. There is a sub array with a phased feed network placed in the middle of the model and it is surrounded by single antennas without a phased feed network to observe the coupling from the sub array to a specific antenna. Feed network phasing means that the signal reaches the antenna [4,2] 26.3° before antenna [3,2] and 52.6° before antenna [2,2], so the radiation and coupling are not symmetric for them, even though surrounding antennas are the same.

The simulation results can be seen in Figures 33, 34, 35, 36 and 37. There it can be seen how the impedance matching of sub array is shifted upwards to 110 MHz without the original isolator elements. Here it does not shift as much as earlier because the ground plane and radome size are now increased to their actual size in the full antenna array. Coupling from the sub array acts similarly as in the last simulation: it is stronger to the antennas in the horizontal direction than to the antennas on the vertical direction or in the corners. However, now the coupling occurs strongest from the sub array to the antennas [2,1], [2,3], [4,1] and [4,3], considering same polarization. The observation of the coupling of the different polarizations shows that it is stronger to a certain column than to another. The polarization 1 of sub array is stronger to the column 1 than to column 3. Further, the coupling from polarization 2 of sub array occurs stronger to the column 3 than to 1. The coupling from the sub array to the antennas located in the vertical direction and the corners was under -25 dB and will not be shown in this thesis to save space.

In Figure 38, the distribution of the E-field on top of the antennas is animated in different phases. This illustrates how each antenna starts to radiate at a different time as the phased feed network conducts a signal to them with a 26.3° phase difference. Here with polarization 1 active, the coupling occurs most to the antenna [4,1] at 3.66 GHz as shown in Figure 33.

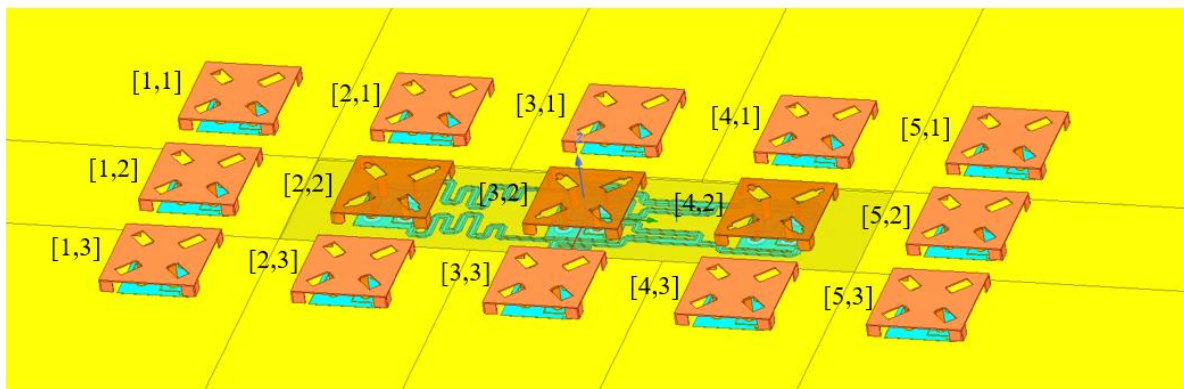


Figure 32. The simulation model to determine the effects of phased feed network.

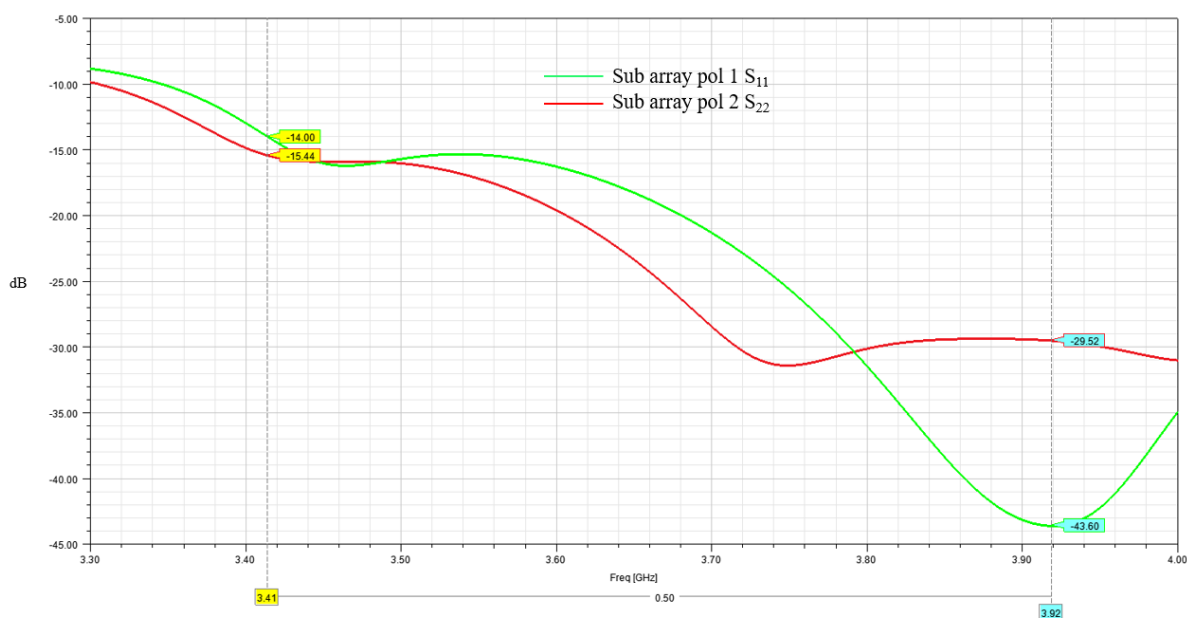


Figure 33. The impedance matching of sub array.

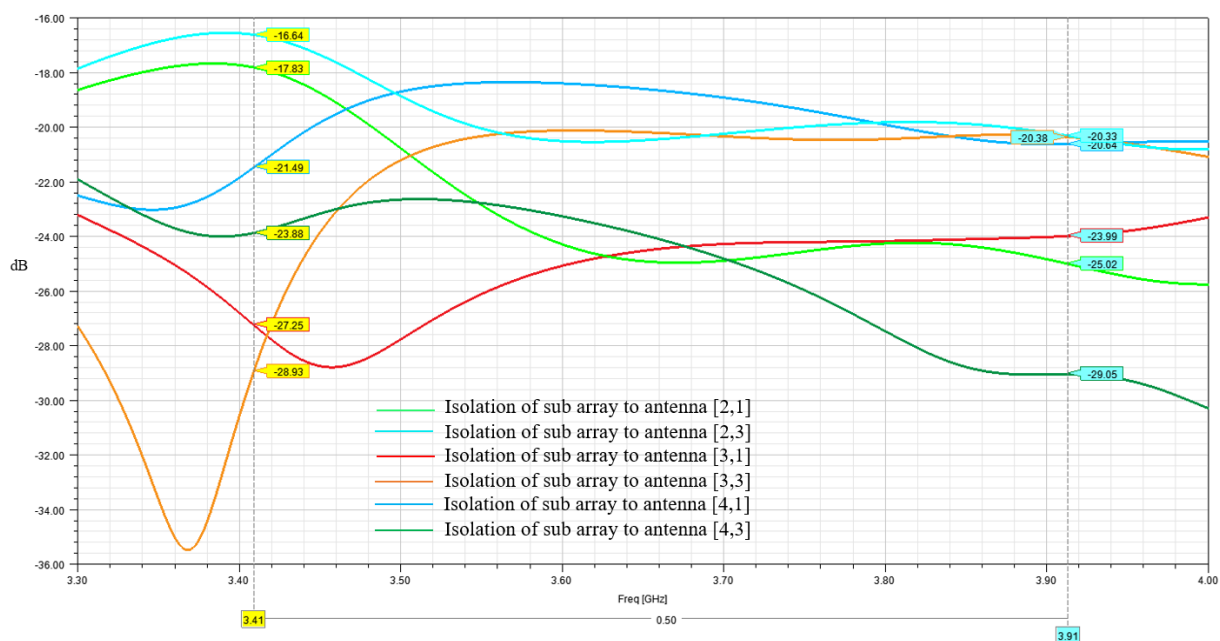


Figure 34. The isolation of the sub array polarization 1 to the antennas in the horizontal direction with the same polarization.

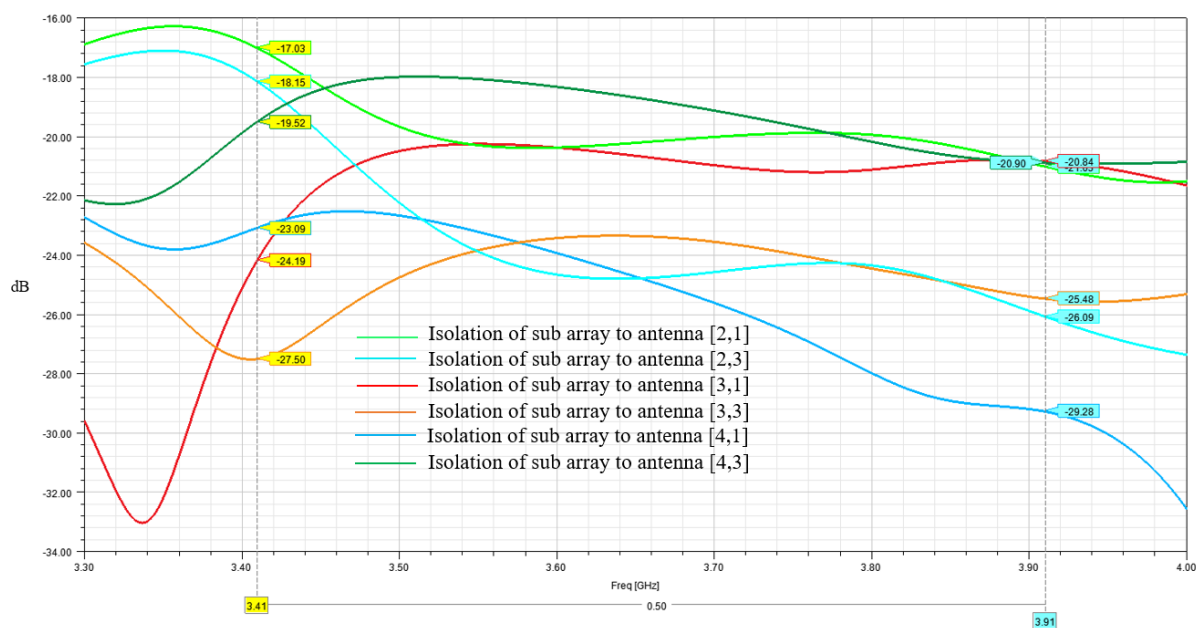


Figure 35. The isolation of the sub array polarization 2 to the antennas in the horizontal direction with the same polarization.

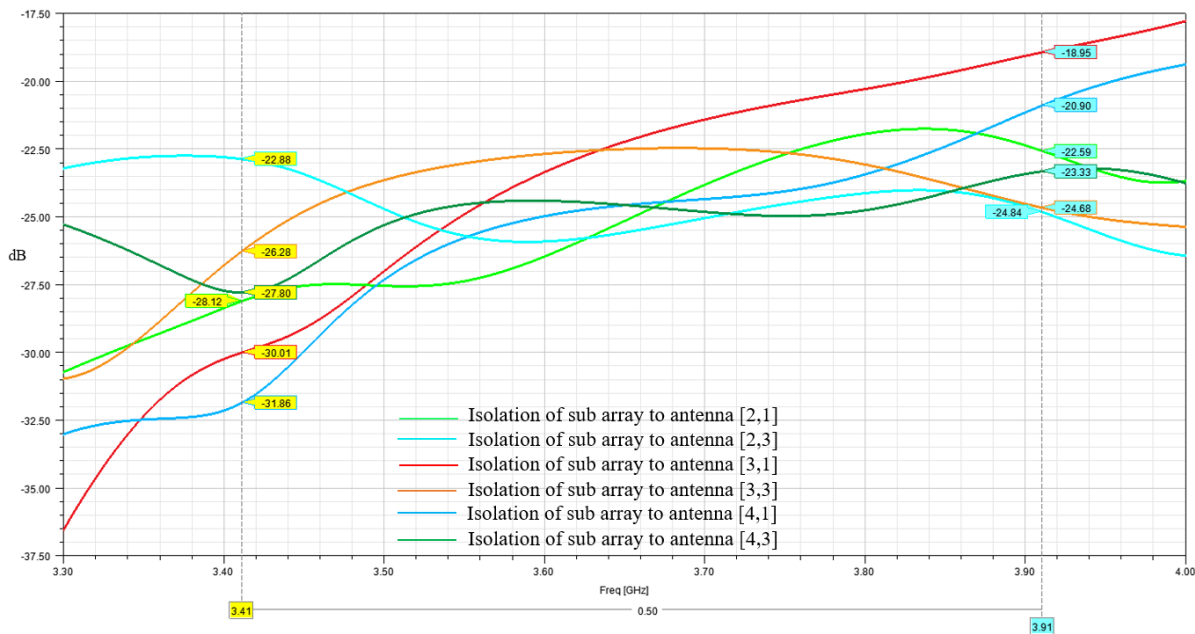


Figure 36. The isolation of the sub array polarization 1 to the antennas in the horizontal direction with different polarizations.

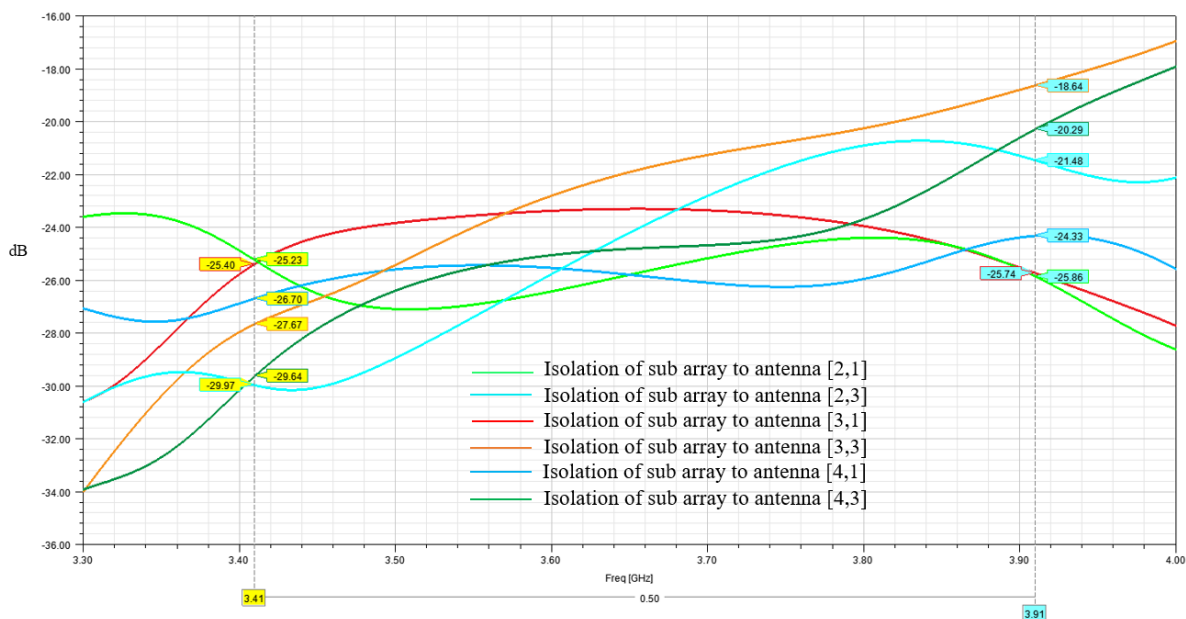


Figure 37. The isolation of the sub array polarization 2 to the antennas in the horizontal direction with different polarizations.

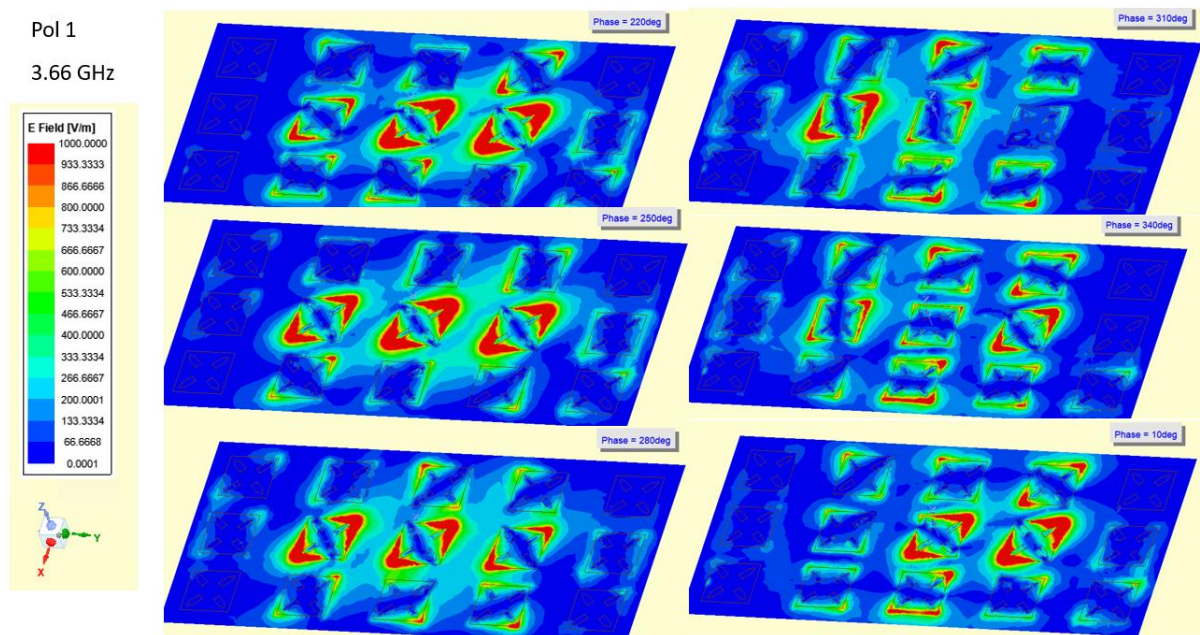


Figure 38. The distribution of E-field on the planar surface on top of the antennas in the small antenna array at 3.66 GHz with only polarization 1 of the sub array active.

5.2.4 Antenna feedline location and orientation

The patch antenna mounted to the plane above ground radiates orthogonally upwards as well as into other directions. To illustrate the radiation from the antennas towards the feedlines and ground of the sub array, E-fields are plotted in Figure 39. There it can be clearly seen how polarization 1 is active and conducts a signal to the antennas. In the different phases of the simulation, the feedline of polarization 1 starts to gather electric charge and it affects the internal coupling of the sub array.

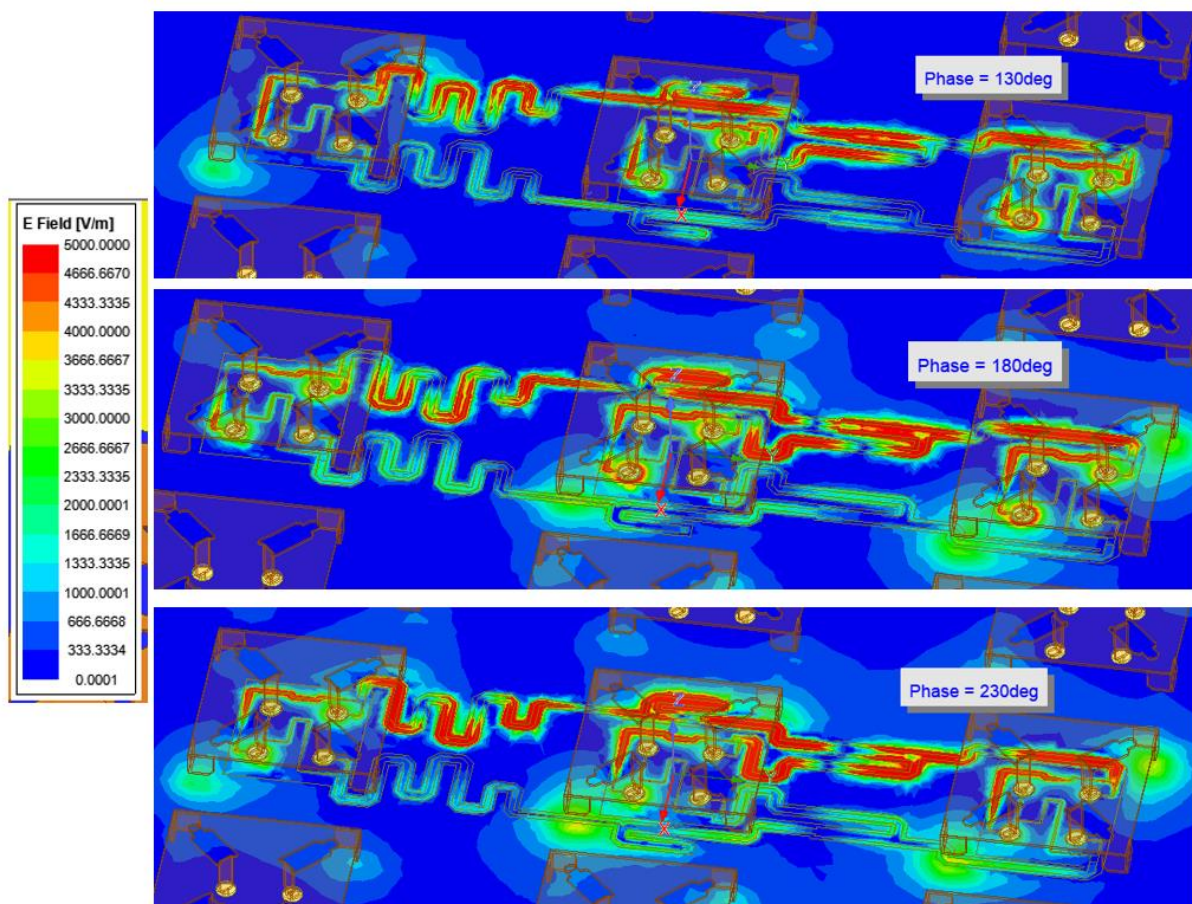


Figure 39. E-fields plotted on the feedlines and ground of the sub array while polarization 1 is active.

Since the patch antenna used in this work is air insulated from the ground, it also radiates towards the ground. To avoid direct internal coupling from the patch to the feedline, the feed network can be mounted on the bottom of the ground plane as in Figure 40. This sub array configuration is simulated as the initial sub array model in Figure 22, so the results are comparable. Impedance matching was almost the same as in the initial design, but as can be seen in the Figure 41 the internal isolation is improved by 1.42 dB. The isolation between the sub arrays is on a very similar level, but the placing of the feedline affects the internal isolation of the model.

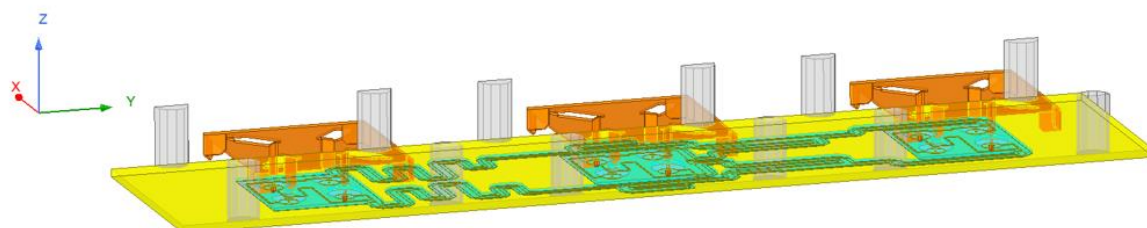


Figure 40. Feed network mounted on the bottom of the ground plane.

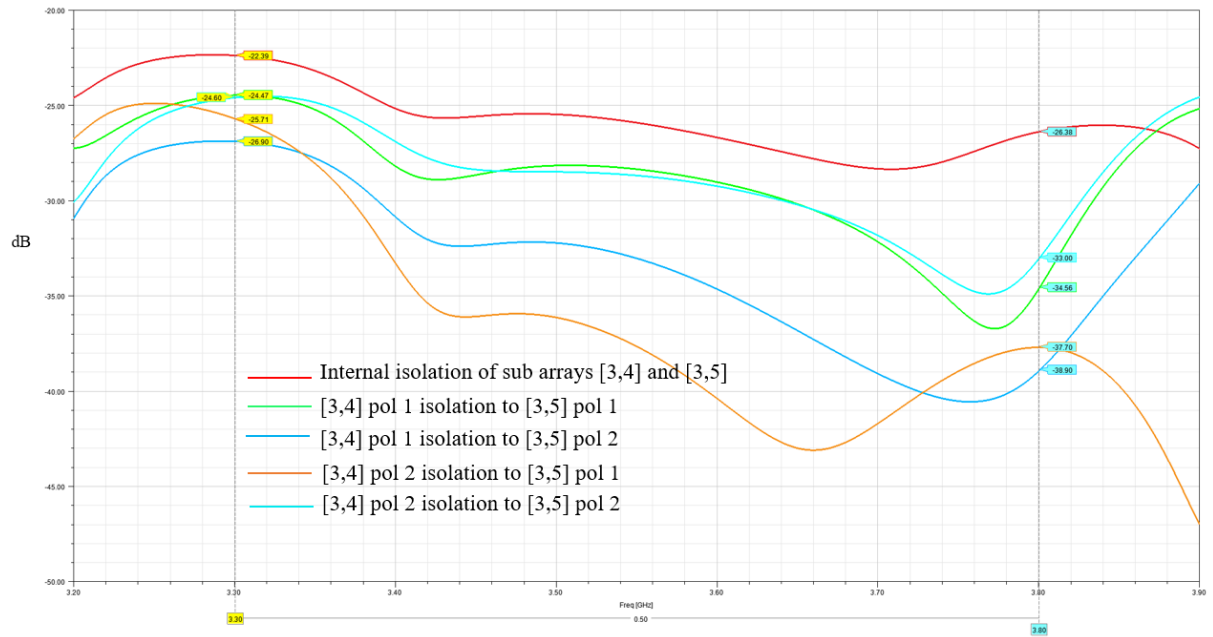


Figure 41. The internal isolation of element [3,4] and [3,5] and isolation between elements [3,4] and [3,5] with the feed network mounted on the bottom of the ground plane.

6 PROPOSED METHOD TO IMPROVE PORT-TO-PORT ISOLATION

As described in the previous chapter, the behaviour of the mutual coupling occurs strongly between antennas in the horizontal direction. The usage of the phased feed network for the sub array provides a -6° vertical radiation pattern pretilt. This causes coupling to be biased more to certain horizontal antennas on than others. Since antennas are placed above the ground plane, they radiate towards the user, other antennas and towards the ground plane. Feedlines placed on top of the ground plane receive this radiation and it causes internal coupling to the antennas. Based on these restricting parameters, the proposed method for the improved port-to-port isolation is designed and simulated as follows: simulating a parameter sweep for the size and position of the isolator structure and observing the results of the matching, isolation and radiation properties to find the most beneficial structure for the isolation without sacrificing matching or radiation properties. In the initial design, the isolator element structure was tubular. Several other structures, such as walls, grids, split ring resonators, were simulated. Additionally, other materials were tested for the walls, but none of these methods were useful for the isolation improvement. During the simulation and analysis phase, it was noticed that adding horizontally wide structures as isolation elements is not beneficial. So, the method to improve port-to-port isolation is proposed and introduced in this chapter. To verify the actual radiation functionality of the proposed method, the radiation properties of the initial antenna array and the proposed method are compared based on the base station antenna standards as explained in this chapter.

6.1 Implementation of proposed method to improve isolation

Several structures and methods were tested during the implementation of the antenna array port-to-port isolation improvement. The best port-to-port isolation performance is provided by the antenna array structure shown in Figure 42. There is a feed network of the antenna array, which is flipped below the ground plane. The initial isolator posts are replaced with similar isolator posts in the corners and sides of the antenna element. Every isolator post has a radius of 1 mm, and they are made of copper. The isolator elements on the corners are placed so that the distance from their centre to the centre of the antenna element are same. The other isolator elements in the corner are placed next to the corner isolators orthogonally to x and y direction and without space between them. The height of the corner isolator elements is 10.5 mm. The isolator elements on side of the antenna in the x and y direction are placed in the middle of the corner isolators and their height is 11.3 mm.

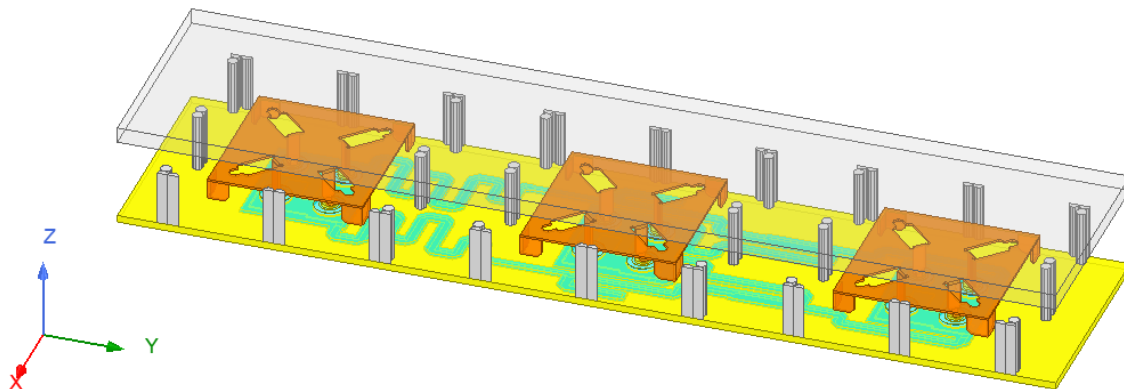


Figure 42. Sub array design for improved port-to-port isolation.

6.2 S-parameter results

The proposed design for the improved isolation is simulated as in the Figure 23 model to compare the isolation results between the proposed and the initial design. The results can be seen in the Figures 43 and 44. The worst isolation is now -23.88 dB and the improved 2.91 dB from the initial design. While simulating the full array, the isolators located on the sides of the antenna in elevation and azimuth direction needed to be modified to fulfil all radiation specifications. In the final design, the isolator elements in the corners remained same, but the height of the isolator elements on the horizontal side of the antennas was reduced to 8 mm and the vertical isolator elements to 4 mm. The final full array design can be seen in the Figure 45. For the full antenna array, the worst port-to-port isolation is -21.58 dB and can be seen in Figure 46. This is a 2.84 dB improvement compared to the initial full array design. For a better perspective, this is double in compared to the original value while observing linear values. In the initial design, the sub arrays located in the sides of the array had the worst internal isolation as illustrated in the Figures 20 and 21. To observe how much these results improved, Figures 47 and 48 illustrate the internal isolation of the sub arrays located in the sides of the array. There is a 4 dB improvement seen when comparing the average results to the initial design.

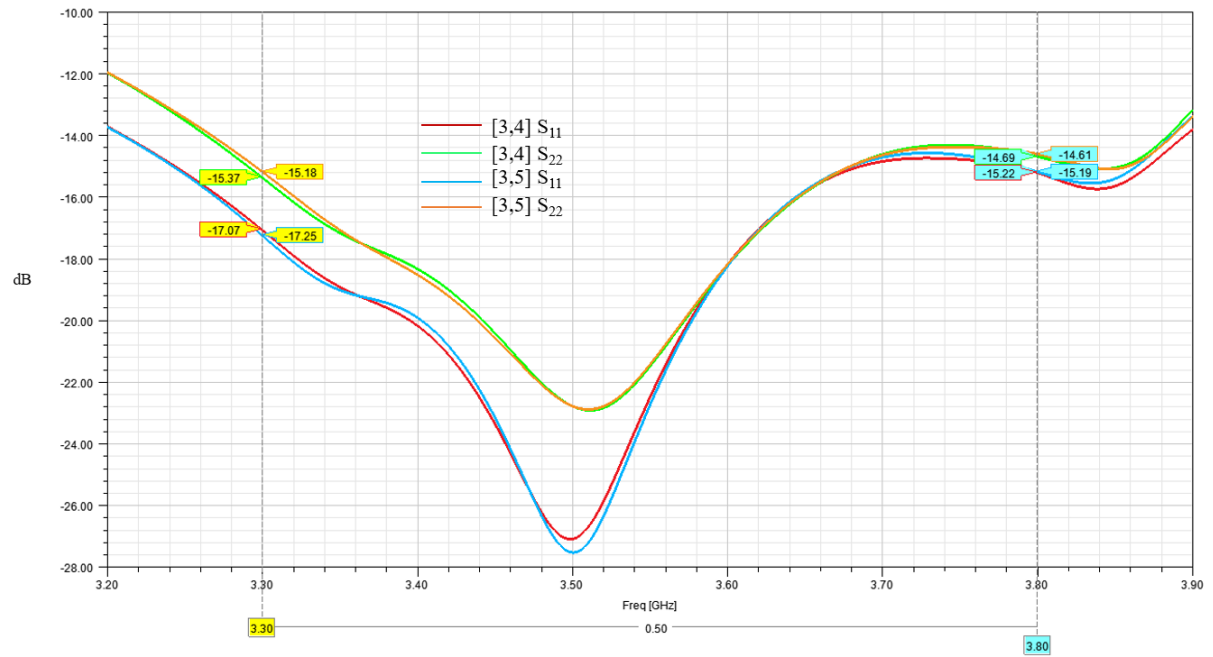


Figure 43. The matching of sub arrays [3,4] and [3,5].

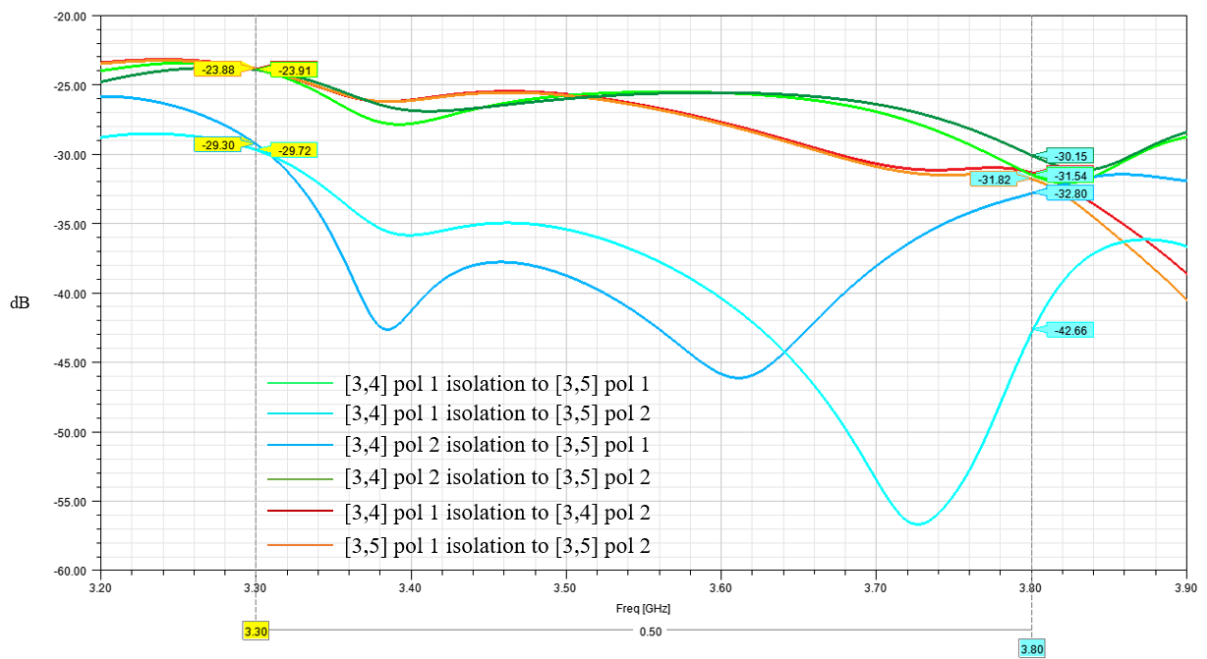


Figure 44. Isolation between sub arrays [3,4] and [3,5].

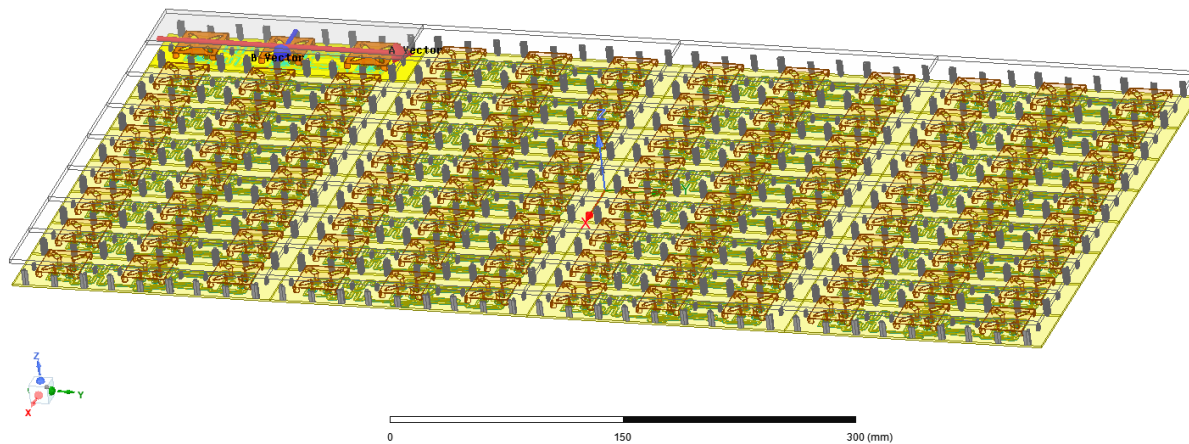


Figure 45. The full array design for the proposed method for isolation improvement.

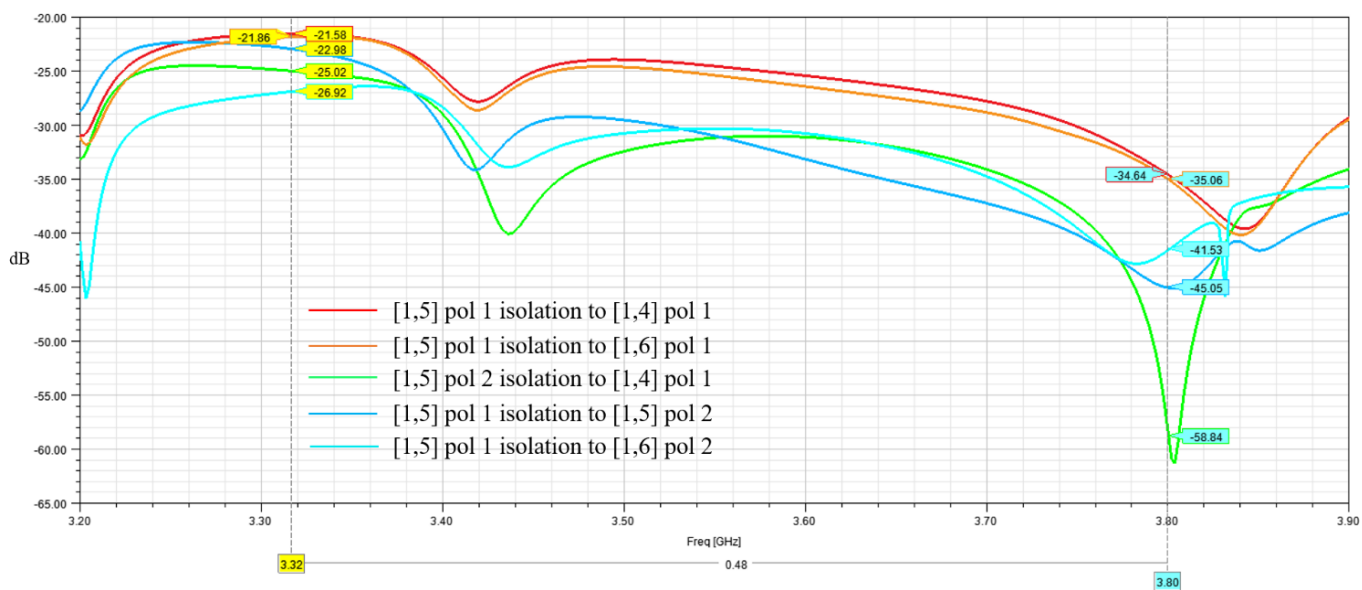


Figure 46. The internal isolation of element [1,6] and the isolation of element [1,5] to element [1,4] and [1,6] considering the same polarization.

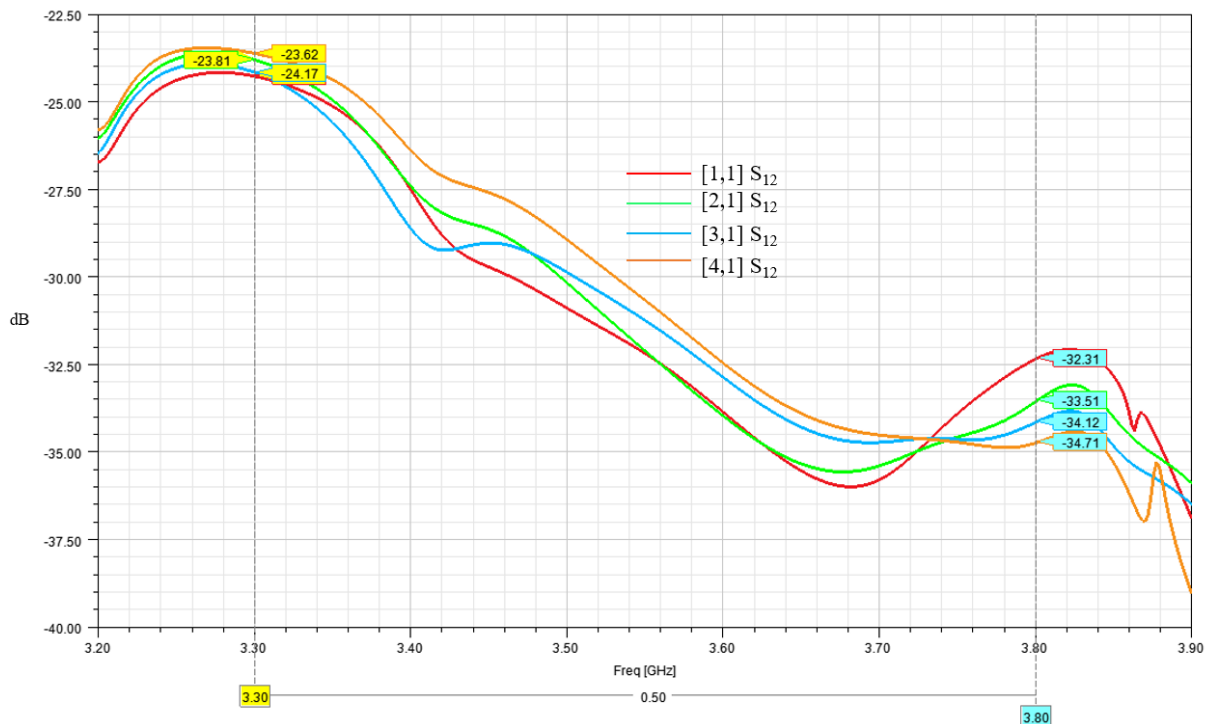


Figure 47. Internal coupling of sub-arrays located in first column.

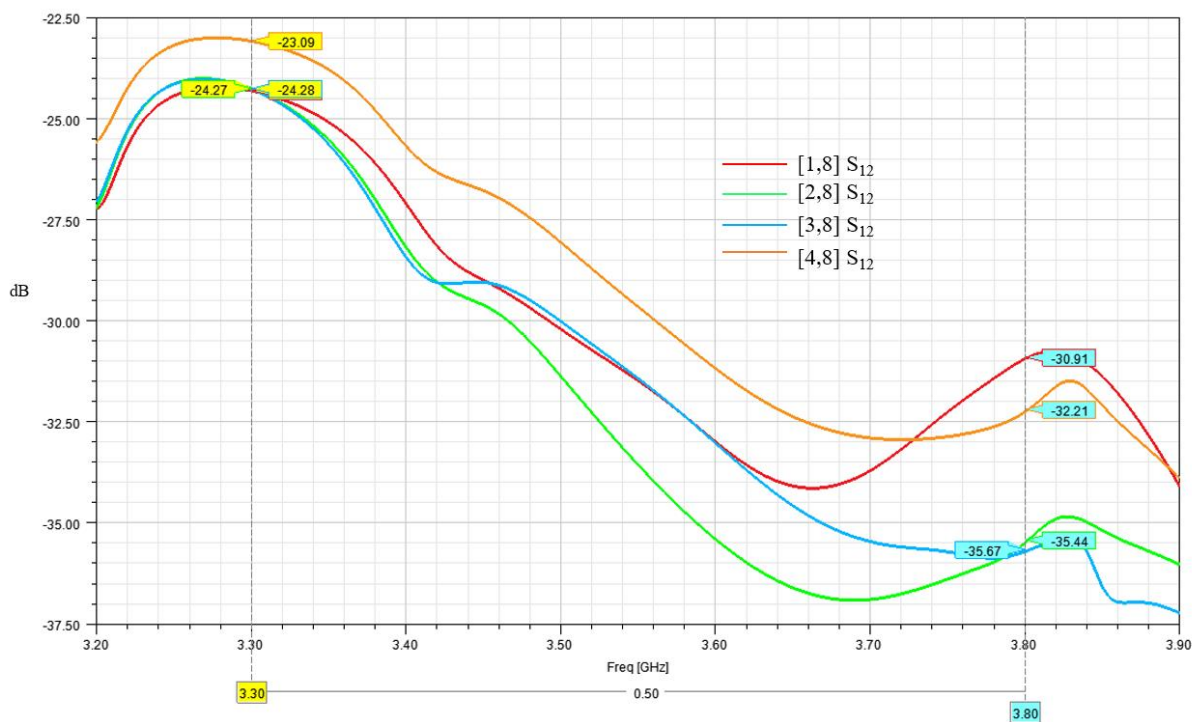


Figure 48. Internal coupling of sub-arrays located in eight column.

6.3 Radiation results

To get more insight of the antenna array radiation functionality, the radiation properties are post-processed with MATLAB software. This means the processing of the whole antenna array radiation results in the far field based on the base station antenna standards. [14] This method

puts the results in order of each specification and removes 16% of the worst results. The mean of the remaining results should meet the requirement. In the Table 1, the specifications, requirements, initial design results, proposed method results, and the difference of these results are covered. There it can be seen how all specifications are passed and most of them are almost same. However, the biggest difference is between the front-to-back ratio and the cross polar discrimination. The front-to-back ratio is reduced by 4.2 dB and cross polar discrimination is improved by 6.7 dB in the electrical boresight and 2.6 over the scanning range, which considers all tilt angles in the specification.

Table 1. Basta analysis

Specification	Requirement	Initial design	Proposed method	Difference
Array beam peak gain, electrical boresight (azimuth cut 0° and elevation cut -6°), dBi	24.0	25.5	25.5	0
Array beam peak gain, elevation tilt range upper limit (azimuth cut 0° and elevation cut -1°), dBi	23.0	24.9	24.7	-0.2
Array beam peak gain, elevation tilt range lower limit (azimuth cut 0° and elevation cut -11°), dBi	24.0	25.0	25.1	0.1
Array beam peak gain, maximum azimuth steering (azimuth cut -50° and elevation cut -6°), dBi	20.0	23.1	23.0	-0.1
Maximum array beam gain drop over 90deg horizontal steering range (azimuth cut -45° and elevation cut -6°), dB	3.0	1.9	1.9	0
Maximum array beam gain drop over 120deg azimuthal envelope beamwidth (azimuth cut -50° and elevation cut -6°), dB	8.0	6.6	6.9	0.3
Minimum azimuth 3 dB beamwidth, electrical boresight (azimuth cut 0° and elevation cut -6°), $^\circ$	13.0, tolerance 1.5	12.9, 0.8	12.8, 0.9	0, 0.1
Minimum front-to-back ratio (azimuth cut -45° and 0° and elevation cut -11° , -6° and -1°), dB	25.0	31.0	26.8	-4.2
Minimum side lobe suppression inside 180° azimuth opening angle, over	8.0	10.6	10.5	-0.1

90° azimuth steering range (azimuth cut 45° and elevation cut -6°), dB				
Minimum grating lobe suppression inside 180° azimuth opening angle, over 120° azimuth steering range (azimuth cut -50° and elevation cut -6°), dB	5.0	8.8	8.7	-0.1
Minimum cross polar discrimination at beam peak, electrical boresight (azimuth cut 0° and elevation cut -6°), dB	20.0	21.4	28.1	6.7
Minimum cross polar discrimination over scanning range (azimuth cut -50°, -45° and 0° and elevation cut -11°, -6° and -1°), dB	10.0	16.4	19.0	2.6
Minimum elevation 3 dB beamwidth, electrical boresight (azimuth cut 0° and elevation cut -6°), °	7.0, tolerance: 1.0	6.2, 0.4	6.2, 0.4	0, 0
Upper side lobe suppression, elevation scanning range (azimuth cut -50° and 0° and elevation cut -11°, -6° and -1°), dB	10	10.9	10.4	-0.5
Lower side lobe suppression, elevation scanning range (azimuth cut -50° and 0° and elevation cut -11°, -6° and -1°), dB	10	11.5	11.6	0.1
Upper side lobe suppression, elevation scanning range (azimuth cut -50° and 0° and elevation cut -13°, -6° and 1°), dB	6.0	8.1	7.9	-0.2
Lower side lobe suppression, elevation scanning range (azimuth cut -50° and 0° and elevation cut -13°, -6° and 1°), dB	6.0	9.4	9.2	-0.2
Array element vertical pretilt deviation from nominal, (azimuth cut 0°), °	3.0	2.5	2.4	-0.1
Array element gain (azimuth cut 0°), dB	9	10.5	10.5	0

Array element vertical 3dB beamwidth (azimuth cut 0°), $^\circ$	20	22.5	21.5	-1.0
Array element horizontal 3dB beamwidth (elevation cut 0°), $^\circ$	75	96.0	97.0	1.0

7 DISCUSSION

The aim of this thesis was to improve the 5G mMIMO antenna array port-to-port isolation performance, while maintaining antenna matching and full array radiation and beam steering properties. The mutual coupling of antennas in the antenna array is a well-known phenomenon in the industry and research community, and thus much research on overcoming it has been done. However, research on the same kind of antenna structure as used in this thesis was hard to find. Most of the research was done for a different antenna structure with smaller array, which utilized a lower bandwidth. Modern 5G base stations need to cover wide bandwidths, which are challenging to design. The design needs to fulfil certain specifications for antenna matching, port-to-port isolation and radiation properties. The high relative bandwidth of this design adds additional challenges for the design work. So, it is safe to say that topic is relevant, up to date on the latest trends on the industry and challenging to implement.

In the initial full array design, restricting port-to-port isolation was mainly the internal isolation of sub arrays located on the sides of the array. The lower sub array is located on the side, the worse isolation gets. A phased array with -6° elevation pretilt makes radiation stronger on the lowest sub array row and sub arrays located on the sides which do not have a symmetrical structure around them. This decreases their internal isolation. Simulations to observe mutual coupling in the initial design were divided into pieces to make observing mutual coupling easier. The coupling between the antennas located in azimuth direction is the strongest because these have the lowest distance between them. Since the actual antenna sub array is fed with phased feed network to fulfil the -6° vertical pre tilt requirement, it changes the coupling between antennas to be more biased to certain antennas in azimuth direction. The usage of the antenna model, which is placed above ground plane, benefits the antenna resonant bandwidth. It also affects the radiation towards ground plane and feed network, which are placed top of ground plane. Antennas couple directly to feedlines and this causes internal coupling to the antenna sub array, which needs to be considered while designing place of feed network.

Based on the restricting factors for mutual coupling, the proposed method to improve port-to-port isolation was designed and simulated experimentally. The feed network of the sub array was placed beneath the ground plane. Parameter sweeps were utilized to find the optimal radius, height, and position for the isolator elements. While optimizing isolation, also antenna matching, and radiation properties were accounted for. To fulfil all radiation specifications for the full array, some of the isolators needed to be shortened. Having isolator elements too high on the elevation direction weakened the cross polar discrimination and pre tilt properties of the full antenna array. This also reduced the worst port-to-port isolation by 1 dB. However, for the final design every radiation property requirement was met, and the worst port-to-port isolation was improved by 2.84 dB.

The initial goal for the full antenna array port-to-port isolation improvement was -30 dB. While making this thesis, it was discovered how challenging it was to achieve. Nonetheless, almost a 3 dB improvement was achieved. It means doubling the original isolation value in the linear scale, which is still a good improvement. Since the specifications for the full antenna array radiation properties were also fulfilled, the results are comparable for the initial design, which adds reliability of the results. The overall reliability of the results depends on the reliability of the simulation tool since the prototype was not built for the proposed method for cost and long component delivery time issues. However, a precisely designed simulation model should match the prototype measurement results well.

If this port-to-port isolation is to be further improved in the future, this thesis gives good preliminary information of how mutual coupling behaves in the design. One method to optimize

port-to-port isolation could be to design sub arrays to be asymmetric since isolation restricts some sub arrays more than others. The strength of the mutual coupling depends on the antenna structure so much that it would be beneficial to do research with different of antenna models, such as dipole, or maybe other innovative models.

8 SUMMARY

This thesis provides a method to improve port-to-port isolation of a commercially deployed 5G mMIMO phased array. The goal of this work was to improve port-to-port isolation in the phased antenna array design of Nokia from -18.74 dB to -30 dB. To fulfil this goal, the occurrence of coupling in the initial antenna design first needed to be understood completely. The basic terminologies of the modern 5G base stations, antenna design properties and mutual coupling as restricting phenomenon are first discussed in the theory sections. Due to the simplicity of the antenna array structures in research papers, it was difficult to find effective methods improving isolation of the phased antenna array model of this work from literature. Most of these research discusses different antenna models, smaller arrays or narrower frequency bandwidths, which results in very different radiation behaviour. Moreover, narrowband coupling mitigation techniques are unsuitable for implementation the wideband antenna array used in this work, which operates from 3.3 to 3.8 GHz. This restricts performance optimization, as every design parameter needs to be fulfilled in wide bandwidth for this design.

The simulation models of this work were created with the electromagnetic simulation software Ansys HFSS and the final design radiation properties were post-processed with MATLAB. To illustrate antenna coupling in the initial design, simulation models were created based on how the coupling occurs. The root causes for isolation performance restrictions were observed prior to the implementation of the chosen methods to improve port-to-port isolation. The worst port-to-port isolation for the proposed method was -21.58 dB, achieving an improvement of 2.84 dB. To verify the radiation properties of the proposed method, these post-processed results were compared to the base station antenna standards. All the results passed the specifications for radiation properties, and these were also compared to initial design radiation results. Almost all of the results were the same, but main changes were related to cross polar discrimination and front-to-back ratio specifications. With the proposed method, cross polar discrimination was improved at the electrical boresight (azimuth cut 0° and elevation cut -6°) and over scanning range (azimuth cut -50° , -45° and 0° and elevation cut -11° , -6° and -1°), while front-to-back ratio was decreased (azimuth cut -45° and 0° and elevation cut -11° , -6° and -1°).

9 REFERENCES

- [1] X. Lin and N. Lee, "5G and Beyond. Fundamentals and Standards," Springer International Publishing, 2021
- [2] Internet site for The World Bank Data (09.09.2022). URL: <https://data.worldbank.org/indicator/IT.CEL.SETS?end=2020&start=1960>
- [3] M. A. Jensen, "A History of MIMO Wireless Communications," IEEE International Symposium on Antennas and Propagation, pp. 681-682, June 2016.
- [4] H. Hu, H. Gao, Z. Li and Y. Zhu, "A Sub 6GHz Massive MIMO System for 5G New Radio," IEEE 85th Vehicular Technology Conference (VTC Spring), pp. 1-5, 2017.
- [5] Nokia white paper (09.09.2022). URL: https://www.rrt.lt/wp-content/uploads/2018/10/Nokia_5G_Deployment_below_6GHz_White_Paper_EN.pdf
- [6] Internet site of European Commission (09.09.2022). URL: <https://digital-strategy.ec.europa.eu/en/policies/5g-research-standards>
- [7] A. Luzatto and M. Haridim, "Wireless Transceiver Design: Mastering the Design of Modern Wireless Equipment and Systems," John Wiley & Sons, 2016.
- [8] C. A. Balanis, "Antenna theory: analysis and design," John Wiley & Sons, 2015.
- [9] G. J. Foschini, "Layered space-time architecture for wireless communication in a fading environment when using multi-element antennas," Bell labs tech. journal, vol. 1 no. 2, pp. 41-59, Autumn 1996.
- [10] T. E. Bogale and L. B. Le, "Beamforming for multiuser massive MIMO systems: Digital versus hybrid analog-digital," IEEE Global Communications Conference, pp. 4066-4071, 2014.
- [11] J. Rahola and J. Ollikainen, "Removing the effect of antenna matching in isolation analyses using the concept of electromagnetic isolation," International Workshop on Antenna Technology: Small Antennas and Novel Metamaterials, pp. 554-557, 2008.
- [12] M. Heino, "Isolation improvement and user-effect modeling for antenna arrays in 5G and beyond," Aalto University publication series, 2020.
- [13] X. Chen, S. Zhang and Q. Li, "A Review of Mutual Coupling in MIMO Systems," IEEE Access, vol. 6, pp. 24706-24719, 2018.
- [14] A. Fournier, "Recommendations on Base Station Antenna Standards," NGMN alliance, March 2019.
- [15] Y. -M. Zhang, Q. -C. Ye, G. F. Pedersen and S. Zhang, "A Simple Decoupling Network with Filtering Response for Patch Antenna Arrays," IEEE Transactions on Antennas and Propagation, vol. 69, no. 11, pp. 7427-7439, November 2021.
- [16] H. Wong, K. -L. Lau and K. -M. Luk, "Design of Dual-Polarized L-Probe Patch Antenna Arrays with High Isolation," IEEE Transactions on Antennas and Propagation, vol. 52, no. 1, pp. 45-52, Jan. 2004.